united nations
educational, scientific
and cultural
organization

international atomic
energy agency

the
abdus salam
international centre for theoretical physics

SMR.1303 - 5

Advanced Course:
CLIMATE CHANGE IN THE MEDITERRANEAN REGION
PART I: PHYSICAL ASPECTS
(12 - 16 March 2001)

"Aerosols in the Mediterranean, their origin and climatic effects"

Emin OZSOY
Middle East Technical University
Institute of Marine Sciences
P.O. Box 28, Erdemli
33731 Icel
TURKEY

In: Malanotte-Rizzoli P. and Eremeev V.N., (editors) The Eastern Mediterranean as a Laboratory Basin for the Assessment of Contrasting Ecosystems, NATO Science Series 2, Environmental Security, v. 51, Kluwer Academic Publishers, Dordrecht, pp. 281-301, 1999.

SENSITIVITY TO GLOBAL CHANGE IN TEMPERATE EURO-ASIAN SEAS (THE MEDITERRANEAN, BLACK SEA AND CASPIAN SEA): A REVIEW

EMIN ÖZSOY
Institute of Marine Sciences, Middle East Technical University, P. O. Box 28, Erdemli, İçel 33731 Turkey

Abstract. Common features of the three relatively isolated Euro-Asian Seas are reviewed to evaluate their sensitivity to climatic or anthropogenic change. The projection of the effects of Global Change occur through physical linkages, mediated by global, basin-scale and meso-scale processes, which need to be better unterstood for better forecasts. Prominent inter-annual / interdecadal signals and large scale controls are evident, and in some cases the changes are of a magnitude detected for the first time in the history of modern observations.

1. Introduction

The Levantine Sea, Black Sea, and the Caspian Sea are the remotest, climatically coupled, progresively isolated interior Seas of the Euro-Asian continent. All three Seas are neighbored by high mountain chains, vast continental flatlands, deserts and fertile lands, in a transition between the Atlantic and Indian Oceans. Ocean-atmosphere-land interactions in this environment of contrasting marine and continental climates, complex land and sea bottom topography, and energetic mid-latitude atmospheric motions make the region prone to extremes, and result in pigment patterns with marked regional differences (Figure 1). As a result, the feedbacks to the global system could be disproportionately large in comparison to the size of the region.

If any property is common among these three Seas, it is their sensitivity to Global Change. Inland seas, with their smaller inertia, respond faster to climatic forcing compared to the global oceans. For the same reason, they are more sensitive to environmental degradation, with the Euro-Asian Seas

Figure 1. Top: Topography of Euro-Asian continent. The Caspian Sea, currently $\sim 28m$ below sea level, shown in blue, bottom: CZCS average pigment concentration (mg/m^3) in the eastern Mediterranean, Black Sea and Caspian Sea regions. Data after NASA/GSFC

being among the most troubled waters of the world ocean (IOC, 1993). Land use / cover and subsequent hydrological changes in the adjacent lands lead to desertification and scarcity of water (Moreno and Oechel, 1995; Jeftic, 1992, 1996; Glanz and Zonn, 1997), amplified by cultural and socio-economic contrasts in the region.

At present the causal relationships explaining the evolution of the ocean-atmosphere system projected onto the region are not well established. Often the changes are mediated through sub-basin and meso-scale processes, and are therefore difficult to be identified.

2. Large-Scale Controls

The region is one of the foremost areas of the world where interannual and long term climatic variability is predominant. In the Mediterranean region such variability is well known (*e.g.* Garrett *et al.*, 1992; Robinson *et al.*, 1993; Malanotte-Rizzoli and Robinson 1994; Jeftic et al., 1992, 1996). The Mediterranean variability appears correlated with global teleconnection patterns, and coupled with the Indian Monsoon system and El Nino / Southern Oscillation (ENSO) (Ward, 1996). For example, good correlation has been found between heavy rain and snow in Israel during the last 100 years and ENSO (Alpert and Reisin, 1986). Similarly, global versus regional climate interaction has been emphasized in the case of the Caspian Sea (Rodionov, 1994) as well as in the Black Sea (Polonsky *et al.*, 1997).

Weather in Europe, extending well into Eurasia, is to a large extent determined by conditions in the North Atlantic, and in particular the North Atlantic Oscillation (NAO) quantified by the normalized anomaly of the sea level pressure difference between the Azores and Iceland (Hurrell, 1995). Severe weather in Europe occurs when the NAO index is positive. The NAO accounts for about one third of the hemispheric interannual variance, and accounts for surface temperature changes as well as evaporation-precipitation anomalies in the European and the Eastern Mediterranean regions (Hurrell, 1995, 1996; Marshall, 1997). It has been linked to sea level changes in the Caspian Sea (Rodionov, 1994), to Danube river runoff directly influencing Black Sea hydrology (Polonsky *et al.*, 1997), as well as to surface winter temperatures, precipitation and river runoff in Turkey (Cullen, 1998).

Large scale control is well expressed in long range atmospheric transport patterns, suggested by the simultaneous occurence (Li *et al.*, 1996; Andreae, 1996) and parallel dependence on the interannual NAO patterns (Moulin *et al.*, 1997) of the transport of aerosol dust from the Sahara desert into the Mediterranean and tropical Atlantic regions. An exceptional case studied during the first half of April 1994 (Özsoy *et al.*, 1998b; Kubilay *et al.*, 1998), has illustrated the role of large scale controls. Atmospheric blocking in the Atlantic had triggered upper air jet interactions and meridional circulations on a hemispherical scale (Figure 2a-c). These interactions resulted in large scale subsidence and cyclogenesis resulting in an anomalous pattern of dust simultaneously transported towards the subtropical Atlantic and the eastern Mediterranean regions, leading to maximum dust concentrations in 30 years of measurements in Bermuda and similarly high values in Erdemli (Özsoy, *et al.*, 1998). It is most interesting that the average sea level pressure was characterized with the typical dipole pattern of the NAO (Fig 2d), with a corresponding high index value of $\sim$4, suggesting

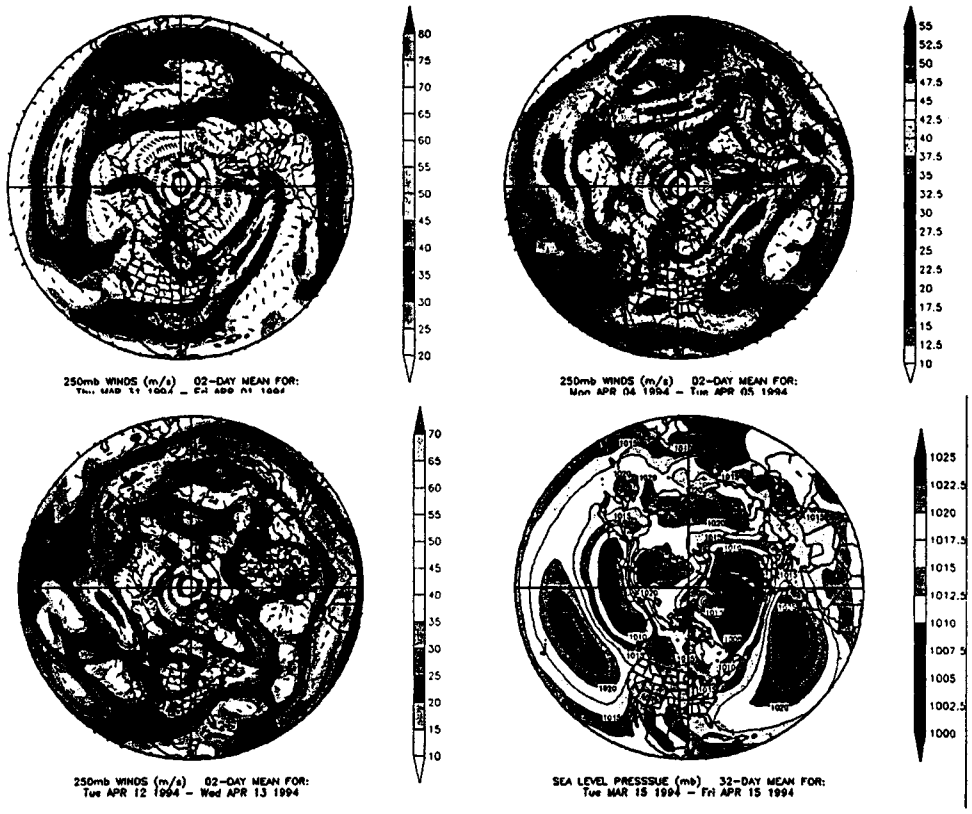

Figure 2. Northern hemisphere upper atmospheric circulation showing the evolution of the polar and subtropical jets. $250hPa$ wind speed (shading) and direction (vectors) based on two day averages for (a) March 31 - April 1, (c) April 4 - 5, 1994, (c) April 12 - 13, 1994 and (d) the monthly average sea level pressure for the priod March 15 - April 15, 1994. The source for the data is NOAA Climate Diagnostic Center (plotting page web adress http://www.cdc.noaa.gov/HistData/

significant links between high index NAO circulation and the anomalous dust event. In addition to the links with NAO, the Atlantic dust flux also appears well correlated with the African drought and the ENSO (Prospero and Nees, 1986).

3. Similarities in Regional Cooling Patterns

There is a significant degree of synchronism displayed between the Levantine, Black and Caspian Seas, in terms of the air and sea surface temperatures displayed in Figure 3. This is because of the proximity of the three regions, but also a result of the possible large scale controls discussed above, and by Özsoy and Ünlüata (1997). In the same Figure, comparisons are also made with the NAO and SO indices and with solar transmission (an indicator of volcanic dust in the atmosphere). Some cold years appear

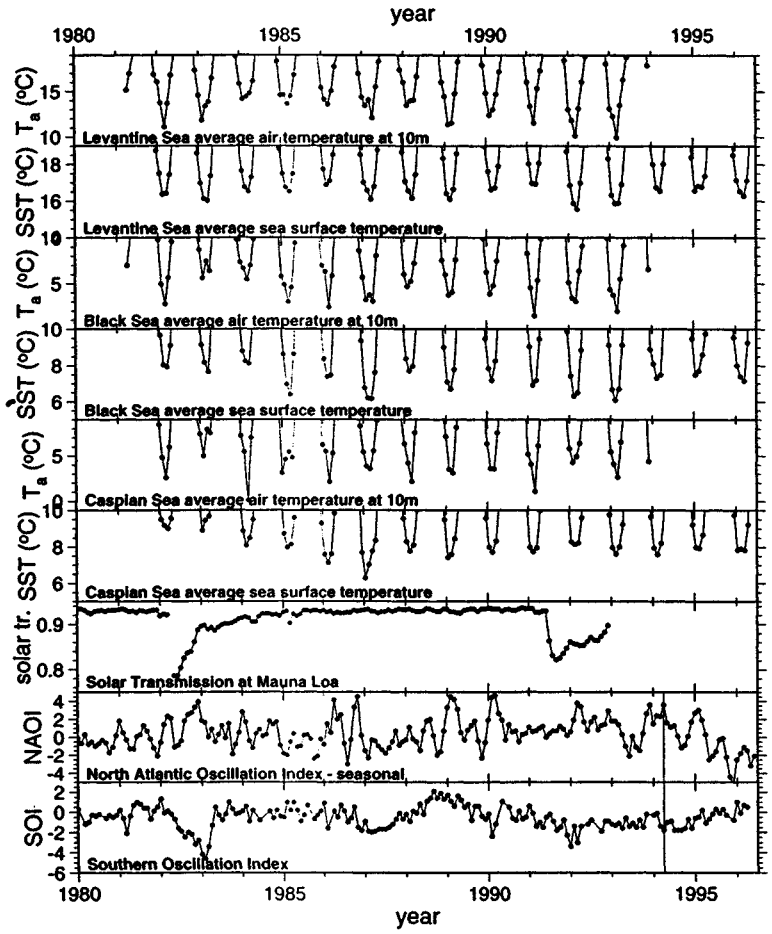

Figure 3. Time series of average air (ECMWF/ERA re-analyses, 6 hr forecast temperature at 10*m* height) and sea surface temperatures (ESA ERS1/ATSR derived monthly averages) for the Levantine, Black and Caspian Seas, Solar transmission at Mauna Loa, and the climatic indices NAOI (seasonal averages) and SOI, for the last two decades.

linked with negative values of the SO Index in Figure 3 (*e.g.* 1982-83, 1986-87, the 1990's), often cited as ENSO years (*e.g.* Meyers and O'Brien, 1995). Similarly, some years (1983, 1986-87, 1989-90, 1992-93) are characterized by high NAO indices.

Relatively cooler winters are detected in the years 1982-83, 1985, 1987, 1989, 1991 and 1992-93 in Figure 3. Some of the cold years correspond to well known cases of convection and deep water formation in the regional seas (*e.g.* from recent data *in 1987*: dense water intrusion into the Marmara Sea from the Aegean, Beşiktepe *et al.*, 1993; deep water formation in the Rhodes Gyre region, Gertman et al., 1990; main pycnocline erosion in the Black Sea, unpublished data; *in 1989*: extensive LIW formation in the

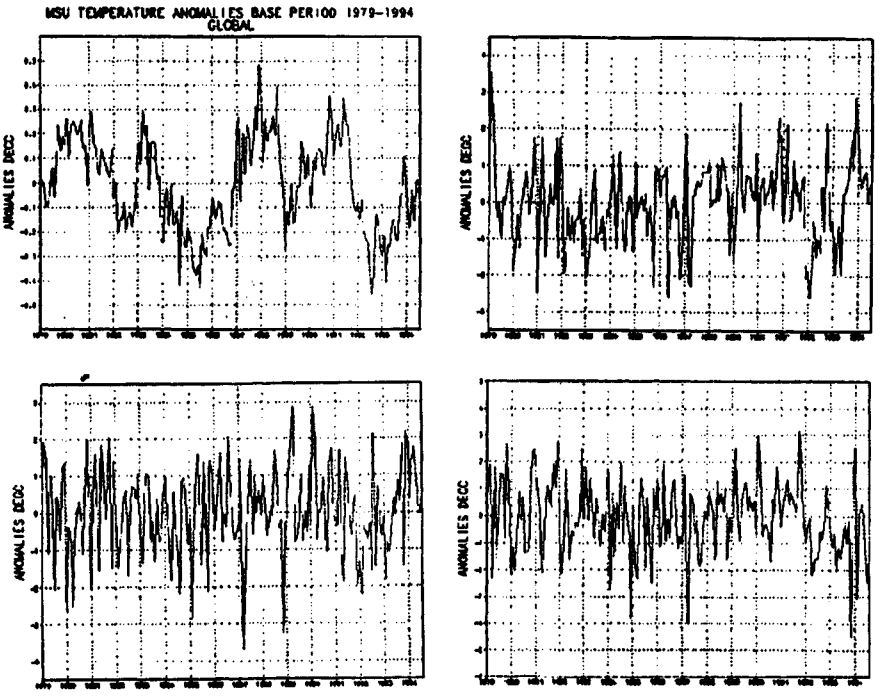

Figure 4. Average lower tropospheric temperature anomalies for (a) the globe, (b) the Rhodes Gyre region of the Levantine Sea (33°-37°N and 26°-32°E), (b) southwest Black Sea (41°-43°N and 27°-31°E), (c) northern Caspian Sea (45°-47°N and 48°-53°E). The measurements were obtained from the Microwave Sounding Unit (MSU) for the 0-5.6km layer of the troposphere (grid resolution 2.5°) and the anomalies calculated over the base period of 1979-1995 are produced by the Global Climate Perspectives System (GCPS) at the http://www.ncdc.noaa.gov/onlineprod/prod.html web address.

northern Levantine Sea (Özsoy *et al.*, 1993); *in 1992 and 1993*: Black Sea Cold Intermediate Water (CIW) formation and pycnocline erosion, Ivanov *et al.*, 1997a,b; simultaneous intermediate and deep water formation in the Rhodes Gyre region of the Levantine Sea; Sur *et al.*, 1992, Özsoy *et al.*, 1993). There are also some surprises: the year 1987 is one of the coolest years in all three seas, but there is no corresponding decrease of air temperature in the Caspian Sea. Secondly, while the air temperature displays various anomalous years in the Caspian Sea, the sea surface temperature does not respond to it very effectively, except the year 1987, unlike the pattern observed for the other two seas.

Cooling in the lower troposphere (Figure 4a) occurred globally in 1992-1993 (Spencer and Christy, 1992), following other cooling periods of 1982, 1985-86, 1989 in the last two decades. Significant drops of Temperature

drops of 1-2°C occurred in the entire region extending from the Rhodes Gyre of the Levantine Sea to the southern Black Sea and the northern Caspian Sea (Figures 4b-d). An event of global climatic significance (Fiocco *et al.*, 1996) the eruption of Mount Pinatubo volcano in June 1991, resulting in stratospheric warmings (Angell, 1993), decreased solar energy inputs (Dutton and Christy, 1992; Dutton, 1994) and anomalous temperatures (Halpert *et al.*, 1993; Boden *et al.*, 1994) in the entire northern hemisphere in 1992-93. Anomalous cold temperatures appeared in the Middle East in very similar spatial patterns during the winters of 1992 and 1993, covering the Black Sea, eastern Mediterranean, and African regions in both years (Özsoy and Ünlüata, 1997). In Turkey, the winter of 1992 was the coldest in the last 60 years (Türkeş *et al.*, 1995), and in Israel, it was the coldest in the last 46 years (Genin *et al.*, 1996).

4. Surface Fluxes

To study the effects of climate variability in the three seas, the loss terms of the surface fluxes are computed from uniform quality, decadal atmospheric re-analysis data obtained from the ECMWF at 1° resolution (mean sea level pressure, $10m$ wind, $2m$ atmospheric and dew point temperatures and cloudiness, produced every 6 hr intervals from $6hr$ global forecasts), and monthly average sea surface temperature based on ERS1/ATSR satellite data for the period 1981-1994. The air-sea fluxes are calculated by a method of iteratively reconstructing the atmospheric variables at $10m$ height from ECMWF supplied fields based on Monin-Obukhov turbulent boundary layer theory, then using bulk formulae to compute the wind-stress, moisture flux, sensible (q_s) and latent (q_l) heat fluxes (Launiaien and Vihma, 1990; Vihma, 1995) as well as the longwave radiation (q_b) fluxes (Bignami *et al.*, 1995). The values are then averaged over the sea domain and a month to produce the values in Figure 5, where the standard deviations are also marked.

The comparison of fluxes in the three different seas shows coincidence between the active periods of Black Sea and Levantine Sea, and a lesser degree of sychronism between them and the Caspian Sea. On the other hand, the Black Sea and Caspian Sea momentum fluxes are larger, more seasonal and more variable than the Levantine Sea, where the larger events come in interannual pulses. The sensible heat flux increases from the Levantine Sea to the Black Sea, reaching a maximum in the Caspian Sea.

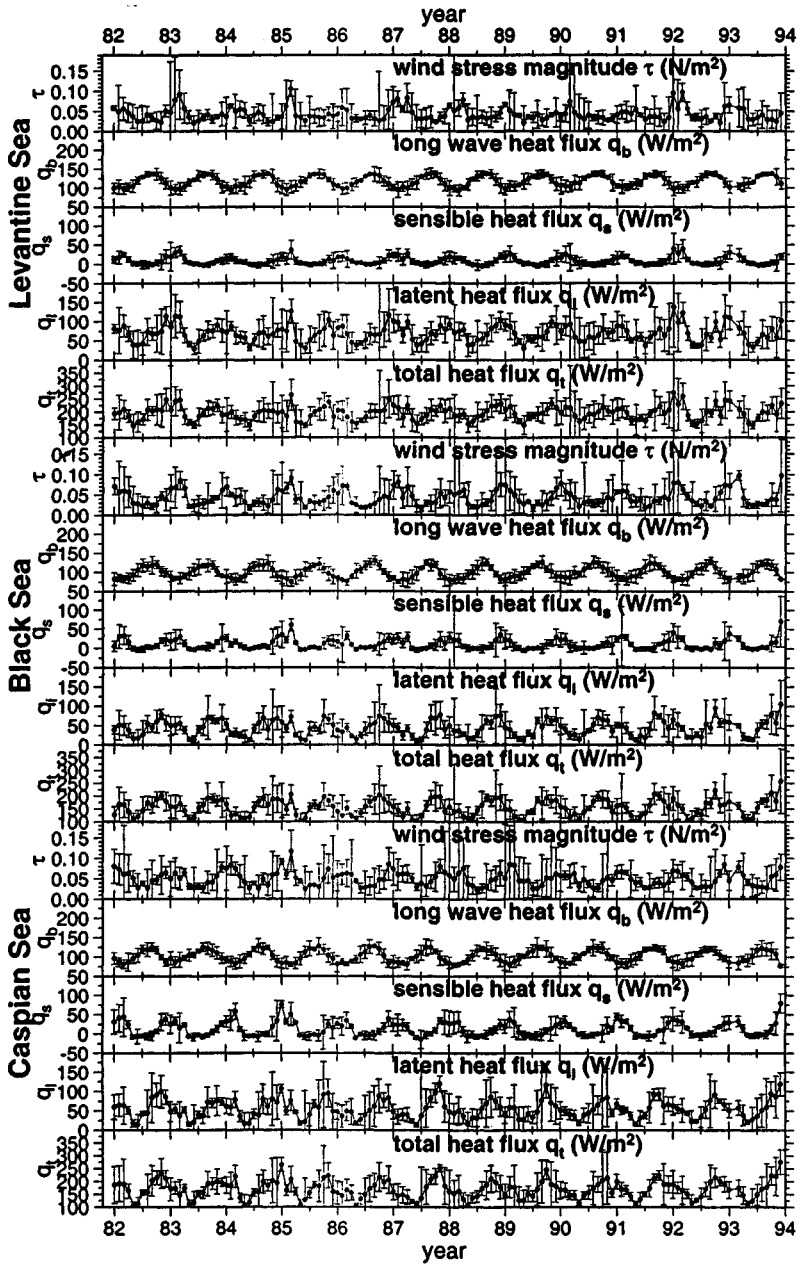

Figure 5. Wind stress and heat flux components for the Levantine, Black and Caspian Seas computed from the ECMWF re-analysis, 6 hourly forecast fields. The values are averaged over each basin and over one month periods. The error bars denote one σ standard deviation.

5. Changes in the Eastern Mediterranean

5.1. THERMOHALINE CIRCULATION

The mean residence time varies considerably from ~100 years for the Mediterranean and shorter for the Caspian, to ~2000 for the Black Sea. The

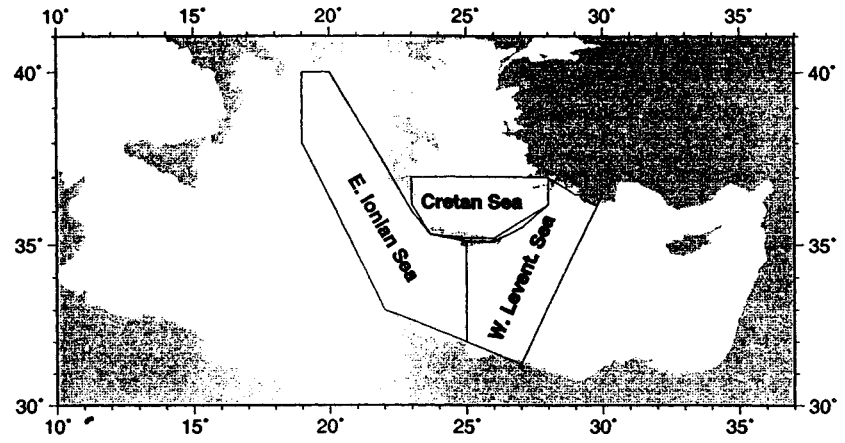

Figure 6. Areas chosen for deep water analyses in the western Levantine, eastern Ionian and Cretan Seas

Mediterranean 'conveyor belt' (*i.e.* the 3-D thermohaline circulation, partly connected to the North Atlantic through the Gibraltar Strait), could have global impact, by regulating water masses and overturning in the North Atlantic (Reid *et al.*, 1994; Hecht *et al.*, 1996), with a potential, yet speculative contribution (Johnson, 1997a,b) to the triggering of paleoclimatic transitions (Broecker *et al.*, 1985).

The conceptual schemes of Mediterranean thermohaline circulations (*e.g.* Robinson and Golnaraghi, 1994) have been drastically changed by the discovery of deep water formation (a) through dense water outflow from the Aegean Sea, and (b) simultaneously with LIW in the Rhodes Gyre core. It is now evident that the 'conveyor belt' circulation in the entire Mediterranean is undergoing changes. Increases in the deep water temperature and nutrients (Bethoux *et al.*, 1989; Bethoux, 1989, 1993) appear coupled to the annual deep convection patterns (Gascard, 1991; Madec and Crepon, 1991; Send *et al.*, 1996) in the western Mediterranean.

The real surprise has recently come from the eastern Mediterranean, where deep water was found to form in the center of the permanent Rhodes Gyre, simultaneously with LIW on its periphery (Gertman *et al.*, 1990; Sur *et al.*, 1992; Özsoy *et al.*, 1993) with a recurrence interval of a few years depending on cooling. Furthermore, a climatically induced switching in the closed cell 'conveyor belt' is now evident. The classical scheme of deep water renewal by dense water (fresh, cold) outflow from the Adriatic Sea (Roether and Schlitzer, 1991; Schlitzer *et al.*, 1991; Roether *et al.*, 1994), have been replaced by the dense water (salty, warm) outflow from the Aegean Sea (Roether *et al.*, 1996), starting in the early 1990's. The event has been detected for first time since the beginning of oceanographic observations,

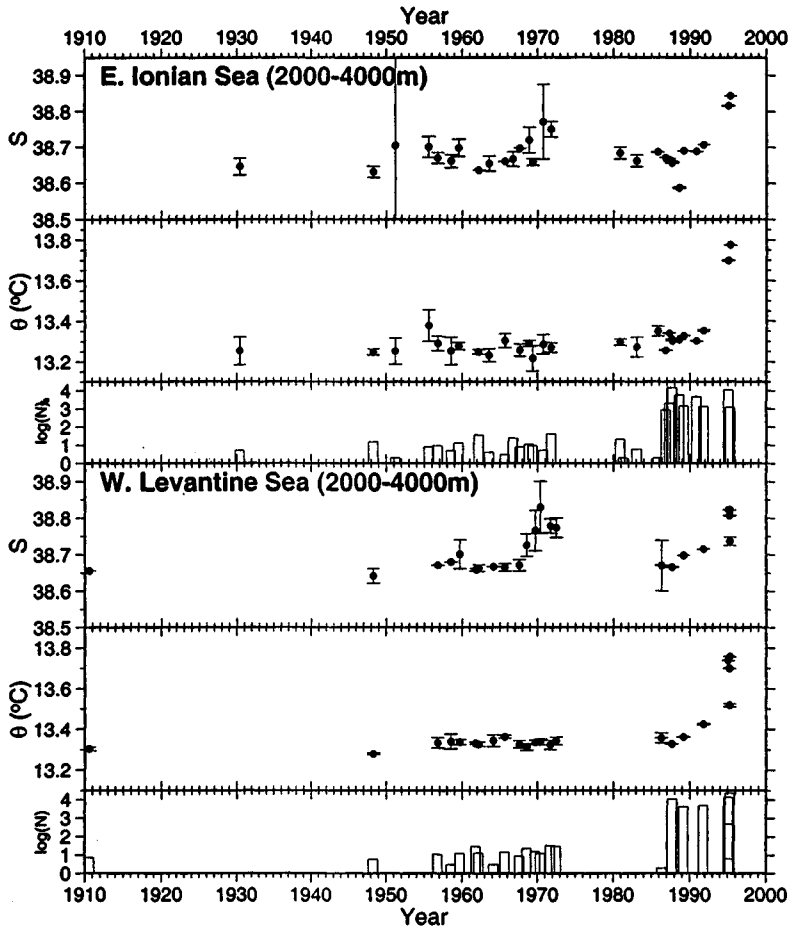

Figure 7. Average salinity, potential temperature, and log number of observations in the depth interval of 2000-4000m in the western Levantine, eastern Ionian Sea areas. The error bars denote standard deviation. The averages are obtained from individual data sets contained within the combined MODB / POEM data and grouped into 1 year intervals falling within the specified depth range.

although intermediate depth ($\sim$ 1,000-1500m) Aegean intrusions of lesser magnitude were well known (Roether and Schlitzer, 1991).

The changes in deep water first became evident when an unusually warm, saline water mass below 1000m was detected south of the Island of Crete during summer 1993 (Heike *et al.*, 1994; A. Yılmaz, pers. comm.). Anomalous heat fluxes were detected in the deep sediments of Ionian Sea deep brine lakes in 1993-94, capped by a double diffusive interface in contact with the new deep water (Della Vedova *et al.*, 1995), suggesting a fresh transient event. Although an exact date for the Aegean dense water outflow can not be established, observations suggest a strong pulse in 1992-93, superposed on a background trend starting in the late 1980's.

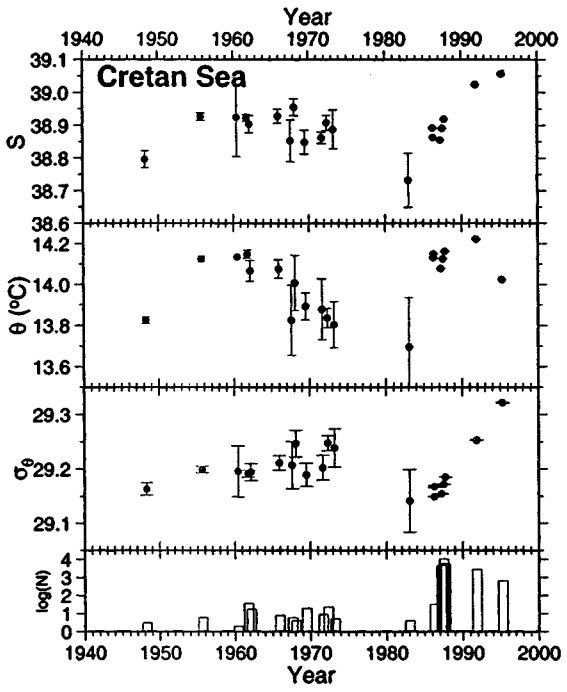

Figure 8. Average salinity, potential temperature, σ_θ density and log number of observations in the depth interval of 1000-2000m in the Cretan Sea. The error bars denote standard deviation. The averages are obtained from individual data sets contained within the combined MODB / POEM data and grouped into 1 year intervals falling within the specified depth range.

An analysis of the MODB historical data base (Brasseur *et al.*, 1996) combined with the last 10 years of Physical Oceanography of the Eastern Mediterranean (POEM) data was made by Özsoy and Latif (1996) to address the effect of Aegean outflow in the observed changes in deep water. For this purpose, the three regions adjacent to the Aegean - Eastern Mediterranean junction (Figure 6) were selected.

The average properties in the depth range of 2000-4000m, with the 95 % confidence limits are shown in Figure 7 the western Levantine and eastern Ionian boxes (Figure 6), together with the number of observations in each annual cluster. The vertical resolution, accuracy and coverage of the measurements increased in the second half of 1980's (POEM program). If we disregard the large salinity changes associated with measurement drift in the 1960's and 1970's, and trust the relatively more accurate temperature measurements, an increase in deep water temperature (and possibly salinity) is evident in both regions in the late 1980's, topped by a rapid increase during 1992-95.

In the Cretan Sea deep water (maximum depth $\sim$2000m), both tem-

perature and salinity have fluctuated at least twice between minimum and maximum values in the last 60 years, starting a steady increase after the mid 1980's (Figure 8). The salinity reached its peak in 1995, while the temperature first increased until 1991 and dropped sharply in 1991-95 to yield a rapid and steady increase in density during the 1980's and 1990's, which is quite different than the relatively constant density values of the previous three decades. Similar conclusions were reached by Theocharis *et al.*, (1996) with regard to Cretan Sea.

5.2. NEAR-SURFACE CIRCULATION

Upper ocean variability has been most readily detected in the circulation of the main thermocline and in the physical properties of the intermediate and surface waters both in the western Mediterranean (Crepon *et al.*, 1989; Barnier *et al.*, 1989) and the eastern Mediterranean (Hecht, 1992; Sur, *et al.*, 1992; Özsoy *et al.*, 1993).

In the eastern Mediterranean, abrupt changes in circulation and water masses has been recognized (Hecht, 1992) as extraordinary, multi-annually recurrent events. The multiple bifurcating central jet flow joining the Asia Minor jet cyclonically east and west of Cyprus and anticyclonically along the eastern coast of Levant in 1985-86 has abruptly changed to a better organized, cyclonic flow around Cyprus in the 1988-1990 period, coincident with the Rhodes Gyre deep convection in 1987, the massive penetration of low salinity modified Atlantic water into the northern Levantine, and the disappearence of a coherent anticyclone in the Gulf of Antalya the same year and its re-appearence in 1990 (Özsoy *et al.*, 1991, 1993). The surface salinity steadily increased from 39.1-39.3 in 1985-86 up to 39.5 in 1989 and 39.7 in 1990. During the same period changes occurred in in the pattern of formation and maintenance of LIW. The LIW trapped in the Antalya anticyclonic eddy in 1985-86 disappeared together with the eddy itself in 1987. LIW with increasingly higher salinities was observed in the winter periods of the following years, reaching from ~39.0 in 1989 to ~39.2 in 1989-90 (Özsoy *et al.*, 1993). An increasing trend was evident in the Shikmona Gyre core salinity, temperature and density during the 1988-1994 period, with abrupt changes in the winters of 1990 and 1992 (Brenner, 1996). Salinity increases in the entire region, together with circulation changes leading to the entry of salt water into the Aegean, and blocking of LIW to spread westward by multi-centered anticyclonic region in the Southern Levantine, have been shown by Malanotte-Rizzoli *et al.*, (1998) for the POEM survey of October 1991. The changes imply a salt redistribution pattern favoring the creation of Aegean dense water outflow.

6. Hydrological Cycles and Sea Level

The sea-level, besides being a good indicator of climatic fluctuations, is a sensitive measure of hydrometeorological driving factors in enclosed and semi-enclosed seas. In the Black Sea, sea-level responds non-isostatically to atmospheric pressure and the total water budget, which are both highly variable on interannual and seasonal time scales (Sur *et al.*, 1994), strictly controlled by the variable inputs of large rivers and the dynamical constraints imposed the Turkish Straits (Özsoy *et al.*, 1998a). Simple models used to understand the time dependent response has had limited success to produce and explain sea-level variations of large amplitude in this non-tidal Sea, unless special effects of wind-setup on the hydraulics of the Bosphorus are included (Ducet and Le Traon, 1998).

In the Caspian Sea, sea-level changes depend on the regional hydrometeorological regime linked to global climate (Radionov, 1994). The sea level changes with climatic and anthropogenic components are of great economic and environmental importance for the surrounding countries. Interestingly, the sea-level change influences the residence time of the deep waters, and therefore has a direct bearing on the health of the Caspian Sea. Abrupt changes in sea-level have occurred twice since 1830's, as well as earlier in history, as the fate of Khazars occupying in its shores in the 10th century stand witness. The sea level has first dropped from a -25 m in 1930's down to -29 m by 1978, and has risen to the present -27 m after 1977. Hydrogen sulfide has been detected in deep waters prior to 1930 when sea-level was high, as a result of insufficient ventilation, limited by the decreased volume of dense water formed on the ice-covered, shallow northern Caspian shelf (average depth $\sim 2m$) under the influence of the large, variable inputs of the Volga river (Kosarev and Yablonskaya, 1994).

7. Marine Ecosystems

The marine ecosystems of interior seas are especially vulnerable, as significant changes in nutrient supplies are taking place in their confined waters. In the Black Sea, and the Caspian Sea, supplied by large rivers, eutrophication is leading to losses of habitats, species diversity, and consequent economical value (Zaitsev and Mamayev, 1997, Kosarev and Yablonskaya, 1994). The eastern Mediterranean system may be undergoing change related to the Nile river (*e.g.* Turley, 1997). Ecosystem disasters in even smaller, confined waters of the the Aral Sea, Kara Boğaz Göl, and Azov Sea, are better recognized. The introduction of extraneous species represent anthropogenic effects, either by filling a niche as in the case of the Black Sea, or through Lessepsian migration from the Red Sea, in the case of the eastern Mediteranean (Por, 1978; Galil, 1993; Gücü *et al.*, 1994;

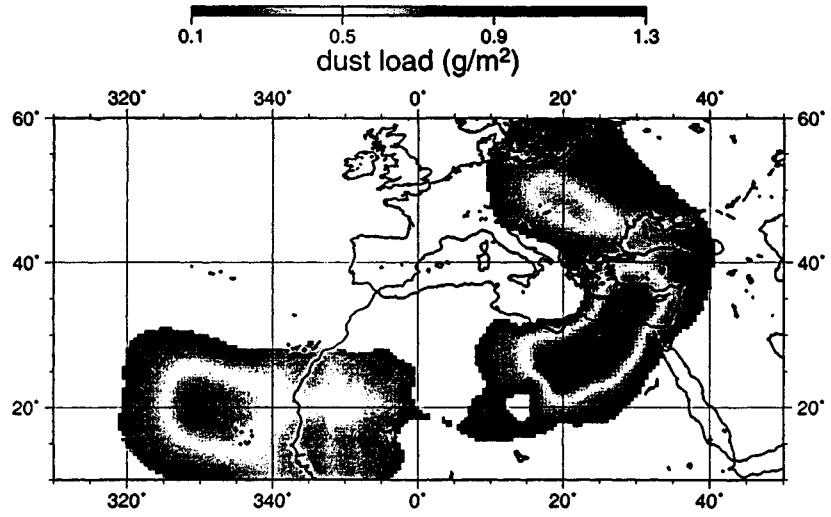

Figure 9. Model derived tropospheric dust load (g/m^2) at 18:00 on April 6, 1994.

Kıdeyş and Gücü, 1995). On the other hand, the natural variabilities are frequently of the same magnitude as anthropogenic effects, which makes diagnosis difficult.

The basic ingredients and biological machinery of the marine ecosystems are often not sufficiently resolved (*e.g.* the sub-oxic zone in the Black Sea, Oğuz, *et al.*, *this volume*; or the roles of P-limitation and cyanobacteria in the eastern Mediterranean, Zohary and Robarts, 1996; Li *et al.*, 1993). In addition to these biochemical factors, dynamical features are of first order importance for the ecosystem. In the Black Sea, upwelling, coastal flows and river supply play important roles (Sur *et al.*, 1994, 1996; Özsoy and Ünlüata, 1997). In the eastern Mediterranean, where the surface nutrients are low, nutrient upwelling at fronts (Özsoy *et al.*, 1993), and nutrient supply in the river mouths and coasts appear significant. Ecosystem changes associated with an uplift of the nutricline following the Aegean dense water outflow are suspected in the eastern Mediterranean (Roether *et al.*, 1996), and are perhaps associated with changes in deep zooplankton (Weikert, 1996). The strong cooling and mixing in 1992-93 produced a massive algal bloom near the Rhodes Gyre (Yılmaz *et al.*, 1996; Ediger and Yılmaz, 1996), and in Eilat, where it lead to the destruction of coral reefs (Genin *et al.*, 1996). These events coincided with the enhanced pycnocline erosion (Ivanov *et al.*, 1997a,b), followed by a massive bloom (Vladimirov *et al.*, 1997) in the following summer of 1992 in the Black Sea. The bloom in the Black Sea apparently produced atmospheric non-sea-salt sulfate aerosols of marine biological origin swept southwards and detected in the Erdemli

measurements (Özsoy *et al.*, 1998c).

8. Aerosol Dust

Aerosol desert dust is important in the climate system, primarily because of its effects on heat budgets (Charlson and Heintzenberg, 1995), especially in semi-enclosed seas (Gilman and Garrett, 1994), on the heterogeneous chemistry of the tropospheric and greenhouse gases (Dentener *et al.*, 1996), as well as on the biogeochemical cycles in the marine environment (Duce *et al.*, 1991).

Dust transport is an important climatic process which is particularly active in the Mediterranean area (Guerzoni and Chester, 1996), with an increasing incidence in recent years associated with drought and desertification. The role of large scale controls in establishing conditions for transport, such as in the spectacular April 1994 case, are outlined in Section 2. The dust load for this unique case of simultaneous transport (Andrae, 1996; Moulin *et al.*, 1997) in a shallow layer across the Atlantic and within a rapidly developing cyclone towards the eastern Mediterranean and Black Sea regions, resulting in anomalously high concentrations in Barbados and Erdemli (Li *et al.*, 1996, Özsoy *et al.*, 1998b; Kubilay *et al.*, 1998) is shown in Figure 9.

Sahara dust is known to be the main source contributing to the formation of the fertile 'red soils' of the eastern Mediterranean. It is hypothesized, based on satellite observations and concurrent dust measurements (unpublished material, IMS-METU) that the transport and deposition on sea surface of eroded dust from the Sahara and Arabian deserts has an impact on short term, episodic phytoplankton blooms in the eastern Mediterranean. There is often a striking coincidence of 'high reflectivity' from the sea surface typically associated with *E. huxleyi* blooms, and the incursions of dust, supported by the coincidence of the fertilization events with high fluxes of carbonates in sediment trap obsetvations. However, the working hypothesis has to be better defined and tested with detailed observations.

9. ACKNOWLEDGEMENTS

This study benefited from a number of activities, most notably the POEM and POEM-BC, international cooperative programs, the NATO SfS Projects TU-FISHERIES, TU-BLACK SEA and TU-REMOSENS projects, as well as other work carried out by the IMS-METU. Special thanks are for the Turkish General Directorate of Meteorology for providing access to the ECMWF data on a collaborative basis.

References

1. Alpert, P. and T. Reisin (1986). An Early Winter Polar Air Mass Penetration to the Eastern Mediterranean, *Mon. Wea. Rev.*, **114**, 1411-1418.
2. Andreae, M. O. (1996). Raising Dust in the Greenhouse, *Nature*, **380**, 389-390.
3. Angell, J. K. (1993). Comparison of stratospheric warming following Agung, El Chichon and Pinatubo volcanic eruptions, *Geophys. Res. Lett.*, **20**, 715-718.
4. Barnier, B., M. Crepon, and C. Le Provost (1989). Horizontal Ocean Circulation Forced by Deep Water Formation. Part II: A Quasi-Geostrophic Simulation, *J. Phys. Oceanogr.*, **19**, 1781- 1793.
5. Beşiktepe, Ş., Özsoy, E., and Ü. Ünlüata (1993). Filling of the Marmara Sea by the Dardanelles Lower Layer Inflow, Deep- Sea Res., 40(9), 1815-1838.
6. Bethoux, J. P. (1989). Oxygen Consumption, New Production, Vertical Advection and Environmental Evolution in the Mediterranean Sea, *Deep-Sea Res.*, **36**, 769-781.
7. Bethoux, J. P. (1993). The Mediterranean Sea, a Biogechemistry Model Marked by Climate and Environment, in: N. F. R. Della Croce (editor), *Symposium Mediterranean Seas 2000*, University of Genoa, Santa Margherita Ligure, pp. 351-372.
8. Bethoux, J. P., Gentili, B., Raunet, J. and D. Talliez (1989). Warming Trend in the Western Mediterranean Deep Water, *Nature*, 347, 660-662.
9. Bignami, F., S. Marullo, R. Santoleri and M. E. Schiano (1995). Longwave Radiation Budget in the Mediterranean Sea, *J. Geophys Res.*, **100**(C2), 2501-2514.
10. Brenner, S. (1996). The Relationship Between Atmospheric Forcing and the Shikmona Gyre, International POEM-BC/MTP Symposium, Molitg les Bains, France, 1-2 July 1996, pp. 87-89.
11. Charlson, R., J. and J. Heintzenberg (1995). *Aerosol Forcing of Climate*, Wiley, 416 pp.
12. Crepon, M., M. Boukthir, B. Barnier, and F. Aikman (1989). Horizontal Ocean Circulatiom Forced by Deep Water Formation. Part I: An Analytical Study, *J. Phys. Oceanogr.*, **19**, 1781-1793.
13. Cullen, H. (1998). North Atlantic Influence on Middle Eastern Climate and Water Supply, *Climatic Change* (submitted).
14. Della Vedova, B., Foucher, J.-P., Pellis, G., Harmegnies, F., and the MEDRIFF Consortium (1995). Heat Flow Measurements in the Mediterranean Ridge Indicate Transient Processes of Heat Transfer between the Sediments and the Water Column (MAST II - MEDRIFF Project), *Rapp. Comm. Int Mer Medit.*, **34**, 100.
15. Dentener, F. J., G. R. Carmichael, Y. Zhang, J. Lelieveld and P. J. Crutzen (1996). Role of mineral aerosol as a reactive surface in the global troposphere, *J. Geophys. Res.*, **101**, 22,869- 22,889, 1996.
16. Duce *et al.* (1991) The atmospheric input of trace species to the world ocean, *Global Biogeochem. Cycles*, **5**, 193-256, 1991.
17. Ducet, N. and P. Y. Le Traon (1998). Response of the Black Sea Mean Level to Atmospheric Pressure and Wind Forcing, (submitted).
18. Dutton, E. G. and J. R. Christy (1992). Solar Radiative Forcing at Selected Locations and Evidence for Global Lower Tropospheric Cooling Following the Eruptions of El Chichon and Pinatubo, *Geophys. Res. Lett.*, **19**, 2323-2316.
19. Dutton, E. G. (1994). Atmospheric Solar Transmission at Mauna Loa, In: T. A. Boden, D. P. Kaiser, R. J. Sepanski, and F. W. Stoss (editors), Trends 93: A Compendium of Data on Global Change, ORNL/CDIAC-65, Carbon Dioxide Information Analysis Center, Oak Ridge, Tenn., USA.
20. Ediger, D. and A. Yılmaz (1996). Characteristics of Deep Chlorophyll Maximum in the Northeastern Mediterranean with respect to Environmental Conditions, *J. Mar. Sys.*, **9**, 291-303.
21. Fiocco, G., D. Fua and G. Visconti (1996). *The Mount Pinatubo Eruption, Effects on the Atmosphere and Climate*, NATO ASI Series, Kluwer Academic Publishers, 310 pp.

22. Galil, B. S. (1993). Lessepsian Migration. New Findings on the Foremost Anthropogenic change in the Levant Basin Fauna, in: N. F. R. Della Croce (editor), *Symposium Mediterranean Seas 2000*, University of Genoa, Santa Margherita Ligure, pp. 307-323.
23. Garrett, C., Outerbridge, R. and K. Thompson (1992). Interannual Variability in Mediterranean Heat and Buoyancy Fluxes, *J. Climatology.*
24. Gascard, J. C. (1991). Open Ocean Convection and Deep Water Formation in the Mediterranean, Labrador, Greenland and Weddell Seas, in: P. C. Chu and J. C. Gascard (editors) *Deep Convection and Deep Water Formation in the Oceans*, Elsevier, Amsterdam, pp. 241-265.
25. Genin, A., Lazar, B. and S. Brenner (1995). Vertical Mixing and Coral Death in the Red Sea following the Eruption of Mount Pinatubo, *Nature*, **377**, 507-510.
26. Gertman, I. F., I. M. Ovchinnikov and Y. I. Popov (1990). Deep convection in the Levantine Sea, *Rapp. Comm. Mer Medit.*, **32**, 172.
27. Gilman, C. and Garrett C., Heat flux parameterizations for the Mediterranean Sea: The role of atmospheric aerosols and constraints from the water budget, J. Geophys. Res., **99**, 5119-5134, 1994.
28. Glantz, M. H. and I. S. Zonn (1997). *The Scientific, Environmental and Political Issues in the Circum-Caspian Region*, NATO ASI Series, 2, Environment - vol. 29, Kluwer Academic Publishers, Dordrecht.
29. Gücü, A. C., F. Bingel, D. Avşar and N. Uysal (1994) Distribution and Occurrence of Red Sea Fish at the Turkish Mediterranean Coast-Northern Cilician Basin. *Acta Adriat.*, **34**(1/2): 103- 113.
30. Guerzoni, S. and R. Chester (1996). *The Impact of Desert Dust Across the Mediterranean*, Kluwer Academic Publishers, Dordrecht, 389pp.
31. Halpert, M. S., Ropelewski, C. F., Karl, T. R., Angell, J. K., Stowe, L. L., Heim, R. R. Jr., Miller, A. J., and D. R. Rodenhuis (1993). 1992 Brings Return to Moderate Global Temperatures, *EOS*, 74(28), September 21, 1993, 436-439.
32. Hecht, A. (1992). Abrupt Changes in the Characteristics of Atlantic and Levantine Intermediate Waters in the Southeastern Levantine Basin, *Oceanol. Acta*, 15, 25-42.
33. Hecht, M. W., W. R. Holland, V. Artale and N. Pinardi (1996). North Atlantic Model Sensitivity to Mediterranean Waters (unpublished manuscript).
34. Heike, W., Halbach, P., Türkay, M. and H. Weikert (1994). Meteorberichte 94-3, Mittelmeer 1993, Cruise No. 25, 12 May - 20 August 1993, (Cruise Report), (Section 5.2.7).
35. Hurrell, J. W. (1995). Decadal Trends in the North Atlantic Oscillation: Regional Temperatures and Precipitation. *Science*, **269**, 676-679.
36. Hurrell, J. W. (1996). Influence of Variations in Extratropical Wintertime Teleconnections on Northern Hemisphere Temperatures, *Geophys. Res. Lett.*, **23**, 665-668.
37. IOC (1993). Priorities for Contaminants in Specific Marine Areas, International Oceanographic Commission, Electronic Library, Information Document INF - 923, Paris, 1 March 1993.
38. Ivanov, L., Ş. Beşiktepe and E. Özsoy (1997a). The Black Sea Cold Intermediate Layer, in: E. Özsoy and A. Mikaelyan (editors), *Sensitivity to Change: Black Sea, Baltic Sea and North Sea*, NATO ASI Series (Partnership Sub-series, Environment, 27), Kluwer Academic Publishers, Dordrecht, pp. 253-264.
39. Ivanov, L., , Ş. Beşiktepe and E. Özsoy (1997b). Physial Oceanography Variability in the Black Sea Pycnocline, in: E. Özsoy and A. Mikaelyan (editors), *Sensitivity to Change: Black Sea, Baltic Sea and North Sea*, NATO ASI Series (Partnership Sub-series, Environment, 27), Kluwer Academic Publishers, Dordrecht, pp. 265-274.
40. Jeftic, L., J. D. Milliman and G. Sestini (1992). *Climatic Change and the Mediterranean*, UNEP, Edward Arnold, London, 673pp.
41. Jeftic, L., S. Keckes and J. C. Pernetta (1996). *Climatic Change and the Mediterranean*, Volume 2, UNEP, Arnold, London, 564pp.

42. Johnson, R. G. (1997a). Ice Age Initiation by an Ocean-Atmosphere Circulation Change in the Labrador Sea, *Earth Planet. Sci. Lett.*, **148**, 367-379.
43. Johnson, R. G. (1997b). Climate Control Requires a Dam at the Strait of Gibraltar, *EOS*, July 8, 1997.
44. Kıdeyş, A. E. and A. C. Gücü (1995). Rhopilema nomadica: a Poisonous Indo-Pacific Scyphomedusan New to the Mediterranean Coast of Turkey, *Israel J. of Zoology*, **41**(4): 615- 617.
45. Kosarev, A. N. and E. A. Yablonskaya (1994). *The Caspian Sea*, Backhuys Publishers, Haague, 259 pp.
46. Kubilay, N., E. Özsoy, S. Nickovic, I. Tegen and C. Saydam (1998). A Hemispheric Dust Storm Affecting the Atlantic and Mediterranean (April 1994): Analyses, Modelling, Ground-Based Measurements and Satellite Observations, (submitted).
47. Launiaien, J. and T. Vihma (1990). Derivation of Turbulent Surface Fluxes - An Iterative Flux-Profile Method Allowing Arbitrary Observing Heights, *Environmental Software*, **5**(3), 113-124.
48. Li, W. K. W., T. Zohary, Y. Z. Yacobi and A. M. Wood (1993). Ultraphytoplankton in the Eastern Mediterranean Sea: Towards Deriving Phytoplankton Biomass from Flow Cytometric Measurements of Abundance, Fluorescence and Light Scatter, it Marine Ecology Progress Series, **102**, 79-87.
49. Li, X., H. Maring, D. Savoie, K. Voss and J. M. Prospero (1996). Dominance of Mineral Dust in Aerosol Light Scattering in the North Atlantic Trade Winds, *Nature*, **380**, 416-419.
50. Malanotte-Rizzoli, P. and A. R. Robinson (editors) (1994). *Ocean Processes in Climate Dynamics: Global and Mediterranean Examples*, NATO ASI Series C: Mathematical and Physical Sciences, vol. 419, Kluwer Academic Publishers, 437 pp.
51. Malanotte-Rizzoli, P., B. B. Manca, M. Ribera d'Alcala, A. Theocharis, S. Brenner, G. Budillon and E. Özsoy (1998). The Eastern Mediterranean in the 80s and in the 90s: The Big Transition in the Intermediate and Deep Circulations (submitted).
52. Madec, G. and M. Crepon (1991). Thermohaline-Driven Deep Water Formation in the Northwestern Mediterranean Sea, in: P. C. Chu and J. C. Gascard (editors) *Deep Convection and Deep Water Formation in the Oceans*, Elsevier, Amsterdam, pp. 241-265.
53. Marshall, J. and Y. Kushnir (1997). A 'white paper' on Atlantic Climate Variability, an unpublished working document.
54. Meyers, S. D. and J. J. O'Brien (1995). Pacific Ocean Influences Atmospheric Carbon Dioxide, *EOS*, **76**(52), 533-537.
55. Moreno, J. M. and Oechel, W., Eds. (1995). *Global Change and Mediterranean Ecosystems*, Springer Verlag, Ecological Studies, **117**, New York, N.Y.
56. Moulin, C., C. E. Lambert, F. Dulac and U. Dayan (1997). Control of atmospheric export of dust from North Africa by the North Atlantic oscillation. *Nature*, **387**, 691-694.
57. Özsoy, E. (1981). *On the Atmospheric Factors Affecting the Levantine Sea*, European Center for Medium Range Weather Forecasts, Reading, U.K., Technical Report No. 25, 30 pp.
58. Özsoy, E., A. Hecht, Ü. Ünlüata, S. Brenner, T. Oğuz, J. Bishop, M. A. Latif and Z. Rozentraub (1991). A Review of the Levantine Basin Circulation and its Variability during 1985-1988, *Dyn. Atmos. Oceans*, **15**, 421-456.
59. Özsoy, E., Hecht, A., Ünlüata, Ü., Brenner, S., Sur, H. İ., Bishop, J., Latif, M. A., Rozentraub, Z. and T. Oğuz (1993). A Synthesis of the Levantine Basin Circulation and Hydrography, 1985-1990, *Deep-Sea Res.*, **40**, 1075-1119.
60. Özsoy, E. and M. A. Latif (1996). Climate Variability in the Eastern Mediterranean and the Great Aegean Outflow Anomaly, International POEM-BC/MTP Symposium, Molitg les Bains, France, 1-2 July 1996, pp. 69-86.
61. Özsoy, E. and Ü. Ünlüata (1997). Oceanography of the Black Sea: A Review of

Some Recent Results, *Earth Sci. Rev.*, 42(4), 231-272.

62. Özsoy, E., Latif, M. A., Beşiktepe, Ş., Çetin, N., Gregg, N. Belokopytov, V., Goryachkin, Y. and V. Diaconu (1998a). The Bosphorus Strait: Exchange Fluxes, Currents and Sea-Level Changes, L. Ivanov and T. Oğuz, editors, Proceedings of NATO TU-Black Sea Project - Ecosystem Modeling as a Management Tool for the Black Sea : Symposium on Scientific Results, Crimea, (Ukraine), June 15-19, 1997.
63. Özsoy, E., N. Kubilay, S. Nickovic and C. Saydam (1998b). A Hemispheric Dust Storm in April 1994: Observations, Modelling and Analyses, XXIIIrd NATO/CCMS International Technical Meeting on Air Pollution, Varna, 28 Sep. - 2 Oct. 1998. (submitted for publication).
64. Özsoy, T., C. Saydam, N. Kubilay, O. B. Nalçacı and İ. Salihoğlu (1998c). Aerosol Nitrate and Non-Sea-Salt Sulfate Over the Eastern Mediterranean, XXIIIrd NATO/CCMS International Technical Meeting on Air Pollution, Varna, 28 Sep. - 2 Oct. 1998. (submitted for publication).
65. Polonsky, A., E. Voskresenskaya and V. Belokopytov, Variability of the Northwestern Black Sea Hydrography and River Discharges as Part of Global Ocean-Atmosphere Fluctuations, in: E. Özsoy and A. Mikaelyan (editors), *Sensitivity to Change: Black Sea, Baltic Sea and North Sea*, NATO ASI Series (Partnership Sub-series 2, Environment, 27), Kluwer Academic Publishers, Dordrecht, 536 pp., 1997.
66. Por, F. D. (1978): Lessepsian Migration - The influx of Red Sea Biota into the Mediterranean by way of the Suez Canal, Springer Verlag, 215 pp.
67. Reid, J. L. (1994). On the Total Geostrophic Circulation of the North Atlantic Ocean: Flow Patterns, Tracers and Transports, *Prog. Oceanogr.*, **33**, 1-92.
68. Reiter, E. R. *Handbook for Forecasters in the Mediterranean; Weather Phenomena of the Mediterranean Basin*; Part 1: General Description of the Meteorological Processes, Environmental Prediction Research Facility, Naval Postgraduate School, Monterey, California, Technical Paper No. 5-75, 344pp, 1979.
69. Robinson, A. R., Garrett, C. J., Malanotte-Rizzoli, P., Manabe, S., Philander, S. G., Pinardi, N., Roether, W., Schott, F. A., and J. Shukla (1993). Mediterranean and Global Ocean Climate Dynamics, *EOS*, 74(44), November 2, 1993, 506-507.
70. Robinson, A. R. and M. Golnaraghi (1994). The Physical and Dynamical Oceanography of the Mediterranean Sea, in: Malanotte-Rizzoli P. and A. R. Robinson (editors), *Ocean Processes in Climate Dynamics: Global and Mediterranean Examples*, NATO ASI Series C: Mathematical and Physical Sciences, vol. 419, Kluwer Academic Publishers, pp. 255-306.
71. Rodionov, S. N., *Global and Regional Climate Interaction: The Caspian Sea Experience*, Water Science and Technology Library, v. 11, Kluwer Academic Publishers, Dordrecht, 256 pp., 1994.
72. Roether, W. and R. Schlitzer (1991). Eastern Mediterranean Deep Water Renewal on the Basis of Chlorofluoromethane and Tritium Data, *Dyn. Atmos. Oceans*, **15**, 333-354, 1991.
73. Roether, W. V. M. Roussenov and R. Well (1994). A Tracer Study of the Thermohaline Circulation of the Eastern Mediterranean, in: P. Mlanaotte-Rizzoli and A. R. Robinson (editors), *Ocean Processes in Climate Dynamics: Global and Mediterranean Examples*, NATO ASI Series C: Mathematical and Physical Sciences, vol. 419, Kluwer Academic Publishers, pp. 371-394.
74. Roether, W., Manca, B., Klein, B., Bregant, D., Georgopoulos D., Beitzel V., Kovacevic, V., and A. Luchetta (1996). Recent Changes in Eastern Mediterranean Deep Waters, *Science*, **271**, 333- 335.
75. Schlitzer, R., Roether, W., Oster, H., Junghans, H.-G., Hausmann, M., Johannsen H. and A. Michelato (1991). Chlorofluoromethane and Oxygen in the Eastern Mediterranean, *Deep-Sea Res.*, 38, 1351-1551.
76. Send, U., J. Font and C. Mertens (1996). Recent Observation Indicates Convection's Role in Deep Water Circulation, *EOS*, 77(7), February 13, 1996, 61-65.

77. Spencer, R. W. and J. R. Christy (1992). Precision and Radiosonde Validation of Satellite Gridpoint Temperature Anomalies. Part II: A Tropospheric Retrieval and Trends During 1979-1990, *J. Climate*, **5**, 858-866.

78. Sur, H. I., Özsoy, E., and Ü. Ünlüata (1992). Simultaneous Deep and Intermediate Depth Convection in the Northern Levantine Sea, Winter 1992, *Oceanol. Acta*, **16**, 33-43.

79. Sur, H. İ., Özsoy, E. and Ü. Ünlüata, (1994). Boundary Current Instabilities, Upwelling, Shelf Mixing and Eutrophication Processes In The Black Sea, *Prog. Oceanog.*, **33**, 249-302.
Sur, H. İ., Y. P. Ilyin, E. Özsoy and Ü. Ünlüata, (1996). The Impacts of Continental Shelf / Deep Water Interactions in the Black Sea, *J. Mar. Sys.*, **7**, 293-320.

80. Theocharis, A., H. Kontoyannis, S. Kioroglou and V. Papadopoulos(1996), International POEM-BC/MTP Symposium, Molitg les Bains, France, 1-2 July 1996, pp. 58-60.

81. Türkeş, M., Sümer, U., and G. Kılıç, 1995. Variations and Trends in Annual Mean Air Temperatures in Turkey With Respect To Climatic Variability, International Journal of Climatology, 15, 557-569.

82. Turley, C. M. (1997). The Changing Mediterranean Sea - A Sensitive Ecosystem ?, Abstracts Volume, International Conference on the Progress in Oceanography of the Mediterranean Sea, EC-MAST Programme, Rome, November 17-19, 1997.

83. Vihma, T. (1995). Atmosphere-Surface Interactions over Polar Oceans and Heteregenous Surfaces, *Finnish Marine Res.* **264**, 3-41.

84. Vladimirov, V. L., V. I. Mankovsky, M. V. Solov'ev and A. V. Mishonov (1997). Seasonal and Long-term Variability of the Black Sea Optical Parameters, in: E. Özsoy and A. Mikaelyan (editors), *Sensitivity to Change: Black Sea, Baltic Sea and North Sea*, NATO ASI Series (Partnership Sub-series 2, Environment, 27), Kluwer Academic Publishers, Dordrecht, 536 pp., 1997.

85. Wallace, J. M. and M. L. Blackmon, Observations of Low-frequency Atmospheric Variability, in: B. J. Hoskins, and R. P. Pearce, *Large-Scale Dynamical Processes in the Atmosphere*, Academic Press, 397 pp., 1983.

86. Ward, N. (1995). Local and Remote Climate Variability Associated with Mediterranean Sea-Surface Temperature Anomalies, European Research Conference on Mediterranean Forecasting, La Londe les Maures, France, 21-26 October 1995.

87. Weikert, H. (1996). Changes in Levantine Deep Sea Zooplankton, International POEM-BC/MTP Symposium, Molitg les Bains, France, 1-2 July 1996, pp. 99-101.

88. Yılmaz A., D. Ediger, Ç. Polat, S. Tuğrul, and İ. Salihoğlu (1996). The Effect of Cold and Warm Core Eddies on the Distribution and Stoichiometry of Dissolved Nutrients and Enhancement of Primary Production and Changes in Elemental Composition of Phytoplankton in the Eastern Mediterranean, International POEM-BC/MTP Symposium, Molitg les Bains, France, 1-2 July 1996, pp. 122-127.

89. Zaitsev, Yu. and V. Mamaev (1997). Marine Biological Diversity in the Black Sea, A Study of Change and Decline, Black Sea Environmental Series, Black Sea Environmental Series, Vol. 3, GEF Black Sea Environmental Programme, United Nations Publications, New York, 208 pp.

90. Zohary, T. and R. Robarts (1996). Experimental Study of Microbial P-limitation in the Eastern Mediterranean, International POEM-BC/MTP Symposium, Molitg les Bains, France, 1-2 July 1996, p. 128.

A Hemispheric Dust Storm Affecting the Atlantic and Mediterranean in April 1994: Analyses, Modelling, Ground-Based Measurements and Satellite Observations

Emin Özsoy
Institute of Marine Sciences, Middle East Technical University, Erdemli, İçel, Turkey

Nilgün Kubilay
Institute of Marine Sciences, Middle East Technical University, Erdemli, İçel, Turkey

Slobodan Nickovic
Euro-Mediterranean Centre on Insular Coastal Dynamics, Valletta, Malta

Cyril Moulin
Laboratoire des Sciences du Climat et de l'Environnement (CEA/CNRS), Gif-sur-Yvette, France

Short title: A HEMISPHERIC DUST STORM ...

in press Journal of Geophysical Research

Abstract.

One of the largest recorded dust tranpsort events originating from the Great Sahara desert during April 1994 affected the entire region extending from the Caribbean to the Eurasian continent. This hemispherical transport of airborne dust took place during a series of storms which developed during the first three weeks of April in a background of low-index circulation. These repeated events are studied through the combined analyses and interpretation of atmospheric data, ground based aerosol measurements, visibility observations, AVHRR and Meteosat visible band satellite data and the results of Eta model simulations including an aerosol transport component. The observations produce a consistent picture of the temporal and spatial development of the dust events, whose main features are used in parts to verify the model results. The rate of dust suspension from some areas of the western Sahara desert exceeded 1.5 $mg\ m^{-2}h^{-1}$ and the maximum column integrated dust load reached 2 $g\ m^{-2}$ during 3-5 April 1994, when the first major suspension event produced two simultaneous pulses of dust moving in opposite directions across the subtropical Atlantic Ocean and the eastern Mediterranean Sea. These dust suspensions were created by surface winds resulting from subsidence on the northeastern side of a blocking anticyclone in the Atlantic region and subsequent winds of an intense developing cyclone in the Mediterranean - African region. In the following period, maximum dust loads of of 4.5 $g\ m^{-2}$ and 2.5 $g\ m^{-2}$ occured respectively on 12 April and 17 April, when new cyclones transported dust across the Mediterranean from Africa to Europe. The generation of the two dust pulses during the first even and the recurrent cyclone transport in the following period are shown to be the result of a large-scale, anomalous atmospheric circulation connected with blocking in the Atlantic Ocean and the interactions of upper air jets downstream of the blocking. The particular state of the hemispheric circulation during the studied period corresponded to the positive phase of the North Atlantic Oscillation (NAO). While previous statistical evidence has consistently linked dust transport in the region with the NAO signatures, we show the same connection based on this case study.

1. Introduction

The aeolian transport of desert dust is an important modifier of climate, through its effects on: backscattering and absorption of solar and terrestrial radiation [*Miller and Tegen*, 1998, 1999; *Tegen et al.*, 1996], the heat budgets of the lower troposphere [*Alpert et al.*, 1998] and the surface layers of the ocean [*Schollaert and Merrill*, 1998] especially in the case of semi-enclosed seas [*Gilman and Garrett*, 1994], greenhouse gases [*Dentener et al.*, 1996], and marine biogeochemistry [*Duce et al.*, 1991, *Guerzoni et al.*, 1999]. The availability and abundance of desert dust in the atmosphere is directly affected by changes in climate [*Tegen et al.*, 1996], and there are indications that the dust events in the Mediterranean region have been increasing in the 1990's [*Avila and Peñuelas*, 1999]. Large scale controls are anticipated. The North Atlantic Oscillation (NAO) is well correlated with Sahara dust events [*Moulin et al.*, 1997]. Sahara dust at Barbados Islands is found to depend on drought conditions and El Niño / Southern Oscillation (ENSO) [*Prospero and Nees*, 1986]. Large scale controls are important in the eastern Mediterranean - Eurasian region, where the coupled land-ocean-atmosphere variability of the various regional seas and the atmosphere appears to have syncronized response to these controls [*Özsoy et al.*, 1999].

Transport of dust from the Great Sahara into the Mediterranean Sea and the Atlantic Ocean tends to occur simultaneously under exceptional cases [*Moulin et al.*, 1997]. For the studied case of April 1994, maximum dust concentrations for the last 30 years were measured at Barbados [*Li et al.*, 1996; *Andreae*, 1996], and for the period 1983-1994 at Sal Island [*Moulin*, 1997], which possibly corresponded to one of the largest of such events in the Eastern Mediterranean, where the record is relatively shorter. The authors experienced the event in Erdemli, on the Mediterranean coast of Turkey, where the screening of the solar radiation produced a marked decrease in visibility and partial darkness during daytime. The maximum measured dust concentration at this site was 1.6 mg/m^3.

Despite their great importance, the typical meteorological conditions leading to dust suspension and transport are difficult to predict or have not been sufficiently well characterized, because they seem to depend on the specific conditions of each region.

Dust is mobilized from the Sahara desert by aeolian processes, and transported to the Atlantic Ocean, Mediterranean-European and Indian Ocean regions (e.g. *Husar et al.*, 1997). The mobilization of dust has seasonal as well as diurnal cycles which depend on source characteristics as well as wind climatology. Results derived from satellite observations [*Husar et al.*, 1997], surface visibility data [*Mbourou, et al.*, 1997] and the fusion of the various sources of data [*Husar and Husar*, 1997] show a seasonal shift in the westward plume of aerosols from the Sahel or sub-Saharan region in winter and

spring, to the central Sahara region at a more northerly latitude in summer. There has been some controversy assigning to either the Sahel region or the Sahara region more weight as the main source region of African dust [e.g. *Mbourou, et al.,* 1997], but finally it seems clear, that the anthropogenically disturbed soils of the Sahel region also have a significant contribution in addition to the Sahara sources. In summer, the transported aerosols are almost twice as large as in winter [*Husar, et al.,* 1997]. The increased numbers of tropical storms and wave disturbances within the tropical easterly jet transport dust from Africa towards the Tropical Atlantic, reaching the Caribbean Sea and north America [*Prospero,* 1981, 1999; *Karyampudi and Carlson,* 1988; *Ott et al.,* 1991, *Perry et al.,*, 1997].

Some Mediterranean dust events have been connected with North African 'Sharav' cyclones [*Alpert and Ziv,* 1989] typically occurring in the winter and spring, and emerging into the Eastern Mediterranean from south of the Atlas Mountains [*Reiter,* 1979; *Brody and Nestor,* 1980]. *Egger et al.,* [1995] have suggested an increase in baroclinicity near the coast as a result of the approach of the polar front in spring, having a major impact upon the formation of Sharav cyclones, successfully incorporated into a dynamical model.

In winter and spring, the Mediterranean Sea is affected by two upper air jet streams: the polar front jet stream (PFJ) originally located over Europe, meanders and affects the Mediterranean region during periods of low index circulation, while the subtropical jet stream (STJ) is typically located over northern Africa. The combined effects of these westerly jets in winter and spring support easterly propagating extratropical cyclone systems as well as frequent cyclogenesis in the Mediterranean - African region *Reiter,* [1975]. One of the important Mediterranean cyclogenesis mechanisms, first suggested by *Reiter,* [1975], later confirmed by *Prezerakos, et al.* [1990] and *Prezerakos,* [1998] is the interactions of the polar front jet stream (PFJ) and the subtropical jet stream (STJ).

Alpert and Ziv, [1989] and *Alpert and Ganor,* [1993] demonstrated a strong relationships between the jet stream and cyclogenesis over north Africa, resulting in the dust plume intrusion in the Mediterranean. A relationship between the jet streams and severe dust storms has also been recognized by *Danielsen,* [1974] in the case of the American continent and by *Tantawy,* [1961] in the the case of the Middle East, who have suggested that the activity of the cyclones leading to dust transport were strongly correlated with the STJ and, in severe weather events, with the southward transition of the PFJ.

We study the spectacular dust storm of April 1994 through analyses of ground and satellite based observations and model simulations. In Section 2 we provide details of the data and methodology used, then in Section 3 we interpret and discuss our results. Section 4 gives brief conclusions and suggestions

for further research.

2. Methodology

2.1. Ground-Based Measurements

Aerosol measurements were available at Erdemli on the Turkish Mediterranean coast (36°N, 34°E, height: $21m$) [*Kubilay and Saydam,* 1995] and at island stations in the tropical Atlantic (Barbados, 13°N, 59°W, [*Li et al.*, 1996] and Sal Island, 16.7°N, 23.0°W, h: $125m$ [*Chiapello et al.,* 1995, 1997]. In the present study, dust concentration is computed from aluminum obtained by elemental analysis at Erdemli, and from silicon concentration at Sal Island.

Horizontal extinction coefficient calculated from standard WMO visibility measurements at meteorological stations were obtained from the Center for Air Pollution and Trend Analysis, Washington University (personal communication, J. Husar).

Rawinsonde data were acquired from the National Climatic Data Center (NCDC) of the National Oceanic and Atmospheric Administration (NOAA).

2.2. Satellite Data

Both the AVHRR visible and infrared data from NOAA satellites as well as the Meteosat satellite were analysed and used for comparisons. The daily composite images in Plate 1 were made by combining Aerosol Optical Depth (AOD) for dust over the ocean obtained from the VIS band of the Meteosat (following *Dulac et al.,* [1992] and *Moulin,* [1997], and Infrared Difference Dust Index (IDDI) over the continent obtained from its IR band (following a simplified version of the method by Michel Legrand). Cloud pixels were then superimposed as seen using the IR band, with white colour denoting the high altitude and grey denoting the low altitude clouds, to visualize weather systems responsible for the suspension and transport processes.

2.3. The Atmospheric Model

The Eta regional atmospheric model, originally developed by the University of Belgrade and the Federal Hydrometeorological Institute of Yugoslavia, with further improvements made by the National Centre for Environmental Prediction, Washington, is used for the simulation of the atmospheric dynamics and dust transport. The model makes use of the numerical techniques and parameterizations as discussed by [*Janjic,* 1977, *Janjic,* 1984, *Mesinger et al.*, 1988, *Janjic,* 1990, *Janjic,* 1994]. The dynamics of the model is based on: large-scale numerical solutions controlled by conservation of integral

properties, energetically consistent time-difference splitting and the step-like mountain representation. The model physics consists of: the viscous sublayer models over water, a turbulence closure scheme based on Kolmogorov-Heisenberg theory, the Betts-Miller-Janjic deep and shallow moist convection scheme, the land surface scheme the grid-scale precipitation scheme and the radiation scheme.

At this level of model development there are several simplification introduced in our model setup. First, we assume that dust particles have uniform size with diameter of 2 μm, simplifying the real particle size distribution. The chosen diameter falls into the interval of dust particles observed to travel longer distances *Perry et al.* [1997] and is well detected by satellite observations. Furthermore, dust concentration is also considered to be chemically passive and a substance that does not affect the atmospheric radiation processes. The radiation effects will be a matter of separate future development, assuming that they cannot significantly modify temperature profiles in our rather short-term model experiments.

The conservation equation for dust is integrated on-line, within the Eta atmospheric model. The dust part of the model describes all the major components of the atmospheric dust cycle. Numerical schemes for advection, turbulent mixing in the free atmosphere and horizontal diffusion of dust are analogous to the schemes used for other scalar variables in the model. Because the detailed description of the model is given elsewhere [*Nickovic and Dobricic,* 1996], and successfully tested in other cases [*Kubilay et al.,* 2000, *Nickovic et al.,* 1997], it is not repeated here. Further development of the model with other applications can be found in [*Nickovic et al.,* this volume].

The surface dust source points in the model are specified according to the *Wilson and Henderson-Sellers* [1984] global 1° x 1° vegetation data set. Vegetation types 70 (sand desert and barren land) and 71 scrub desert and semi desert) are used to define the dust source points in the model. Dust suspension from the earth's surface is a function of the availability at the surface, soil wetness, and the applied wind stress (friction velocity) [*Nickovic and Dobricic,* 1996].

In designing the dust production scheme, the viscous sublayer model is used [*Nickovic et al.,* 1997], exploiting the physical similarity between turbulent mixing over the sea and over deserts [*Chamberlain,* 1983; *Segal,* 1990]. Following the analogy with momentum/heat/moisture surface interchange of the atmospheric parameters, it is assumed that in the case of dust mixing a thin viscous sublayer just above the desert surface sublayer is created under smooth flow conditions. The transition toward the rough flow is happening with the increased turbulent mixing. Under fully developed turbulence, the viscous sublayer vanishes and mobilization and saltation of particles over dust surfaces starts. Under such conditions there is an efficient interchange of dust material between the desert surface and the

atmosphere. Ground wetness effects on dust production are incorporated as well. Once injected into the atmosphere, dust is transferred in the vertical by the vertical advection and vertical turbulent mixing processes. The vertical advection scheme conserves the dust mass and does not produce new maxima. Wet deposition due to precipitation is represented by a scavenging parameterization scheme. The dry deposition scheme takes into account gravitation settling effects.

The present model of dust suspension, transport and deposition has produced reliable results in a number of earlier tests, where the concentration and spatial coverage of dust over the sea have been verified with satellite and ground based dust measurements in the western and eastern basins of the Mediterranean for a number of major dust storms [*Nickovic and Dobricic,* 1996; *Kubilay et al.,* 2000; *Nickovic et al.,* 2000].

The April 1994 dust transport episode was simulated with the model domain covering most of the Sahara and Atlantic, with a resolution of $0.75° \times 0.75°$ (horizontal) and 32 model vertical layers (distributed as 4 levels within the first 250 m, 7 levels within 0.25-1.00 km, 10 levels within 1-5 km and 11 levels within 5-10 km elevations). The model was run from March 28 until April 22 1994 in a sequence of 24 hr simulations. The meteorological part of the model was initialized using the objective analyses of the European Center for Medium-Range Forecasts (ECMWF) with updates every 24 hours. The ECMWF fields were also used in order to specify the model lateral boundary conditions with updates every 6 hours. The model dust fields were updated every 24 hr, based on the previous day's run. The model topography and soil types used to characterize desert areas are shown in Figure 1.

3. Results and Discussion

3.1. Atmospheric Blocking and Jet Interactions

We first describe changes in the hemispherical weather in this section to identify the underlying features of the circulation and wind systems driving peak dust suspension and transport during the period of investigation.

The synoptic situation on April 1, 1994 was characterized by the subtropical high pressure at 35°N 35°W, the subpolar (Icelandic) low pressure at 65°N 10°W, both centered in the Atlantic Ocean, and the equatorial low pressure across the Tropical Atlantic and the African continent. The Siberian high pressure dominated the Eurasian continent, except near the Middle East, where a cyclone had passed in the earlier period. The Central Mediterranean was dominated by high pressure.

During the following period in the first part of April 1994, the hemispheric circulation undergoes an 'index cycle', developing low zonal index (meridional) patterns and repeated cyclone activity that

persist for more than two weeks. In Figures 2 and 3 we show the hemispheric development based on atmospheric data obtained from NOAA Climate Diagnostics Center, whereas the model results displayed later are based on ECMWF data initializations.

The geopotential height field at $500hPa$ pressure level on April 1 (Figure 2a) shows a coherent zonal flow excluding a dipole in the Atlantic Ocean (25°N). This dipole at mid-troposphere is slightly shifted to the south relative to the subtropical anticyclone at the surface (not shown). An inspection of the circulation indicates that the subtropical high pressure pressed towards Spain around April 2-4, and in the following days, the uniform zonal jet at $500hPa$ developed into a low index, meridionally perturbed flow over Europe and the Middle East. On April 4 a cut-off low developed near the eastern part of the Atlas Mountains (35°N 10°E), in the Western Mediterranean Sea. On April 5 (Figure 2b), the cutoff low, marking a deep cyclone, shifted east to about 35°N 18°E on the $500hPa$ geopotential field. The cyclone on the sea-level pressure maps (not shown) later moved north to the Balkans and Eastern Europe through the Gulf of Sirte, reaching the positions 42°N 20°E on April 6, 52°N 22°E on April 7, 60°N 22°E on April 8, and disappearing thereafter. On April 9 (Figure 2c), the meandering of the zonal jet increases and extends from Europe across Asia into the Pacific region. On April 13 (Figure 2d), the low index flow develops further and extends eastwards from the mid-Atlantic region, with a weak jet shifted north of Europe. A cyclone persists over southern Europe and its surface center shifts to western north Africa on April 15, and moves once again over the Mediterranean on April 16. On April 17 the cyclone is evident in the $500hPa$ geopotential height (Figure 2e) and affects north Africa till April 20. During the entire period of investigation, the recurrent cyclone centers follow circular trajectories: after approaching the Eastern Mediterranean from west, they turn north and later west, to be reformed in northwest Europe before moving east. The recurrent cyclones thus form a semi-stationary weather pattern in which the cyclones are diverted north before they are advected east, partially in agreement with the weakened jet flow over Europe observed in the $500hPa$ geopotential fields.

The blocking circulation in the Atlantic region displayed in Figures 2 and 3, evidently having a prominent barotropic component, forces the upper tropospheric jet streams downstream of it to approach each other and come into contact in the following period. This is best displayed by a sequence of daily upper air winds in Figure 3. The shaded areas are the projections of the regions where the upper air speed exceeds 30 m/s, *i.e.* the cores of the polar and subtropical jet streams. During the later part of March and on April 1 (Figure 3a), there are two separate jet streams over the Atlantic and European regions, one located at high and the other at low latitudes; then on April 2 - 4, the two

jets start to interact. On April 5, the zonal jet starts to get deformed and flows towards Africa, while meanders develop near its extension zone over Europe and the Middle East (Figure 3b). During April 5 - 7 the meridional pattern of circulation is further deformed, and the two jets which come into contact in the preceeeding days finally coalesce on April 9 (Figure 3c), to form a single jet extending from the Mediterranean-European region to Central Asia near the Himalaya Mountains. By April 13 (Figure 3d), the subtropical jet becomes more coherent and strong compared to the polar jet, which develops new meanders, but with smaller speed.

Low zonal index circulations in the atmosphere are often associated with 'blocking', when a quasi-stationary air mass blocks and diverts the mean flow, as shown in the April 1994 case. Blocking typically develops in the mid-latitudes, where it is normally least expected (based on destabilizing effects of zonal jets and baroclinicity), and accounts for a considerable portion of the low frequency variability in the atmosphere [*Wallace and Blackmon*, 1983]. Modons, or coherent dipole vortices, arising through nonlinear processes, represent stable patterns (with a high pressure center situated north of a low) embedded in a zonal mean flow that ideally develop blocking conditions [*McWilliams*, 1980; *Flierl et al.*, 1980]. We observe all of the above to be dominating the investigated case.

3.2. Dust Suspension and Transport

A review of satellite derived daily composite images of dust related AOD over the sea and IDDI over land, for the period of interest (Plate 1) show the sources and distribution of consecutive dust events in the Mediterranean and subtropical Atlantic regions through the period. Corresponding to increased momentum transport from the atmosphere towards the ground over the desert areas of Saharan Africa during either subsidence coming from the North Atlantic or cyclonic development in the Mediterranean-African regions, the IDDI shows increased source activity (suspension) in these regions. In Plate 1, immediately after the period of increased IDDI over land, increased amounts of dust in the adjoining Atlantic Ocean and Eastern Mediterranean regions are evident from AOD measured over the ocean, confirming that the dust suspended over the Sahara is transferred to the adjoining ocean regions.

On April 3 and 4 (Plates 1a,b) we find a large area of suspended dust (IDDI) in the western Great Sahara in agreement with the increased fluxes there (cf. Figure 4a), which then moves east across the desert towards the Gulf of Sirte during the following days. On April 5 and 6 (Plate 1c,d), along with a decrease in the activity of the source areas in western Sahara (IDDI), new source areas of dust are formed in the east (cf. Figures 4b,c). The dust cloud in the eastern Mediterranean (IDDI and AOD) is partially masked by the clouds of the developing cyclone between Tunisia and the Gulf of Sirte. During

the same dates the dust cloud in western Sahara moves to the Atlantic where the AOD is increased to reach a peak near Sal Island on April 5 (Plate 1c), verified by ground measurements and model results later (cf. Figure 10). During the initial phase of development on April 3-6 (Plate 1a-d) the spreading of the dust into the subtropical Atlantic is observed to be in the form of a semi-circular arc, suggesting a frontal structure of the dust storm extending into the ocean. On April 6 and 7 (Plate 1d,e), the dust front has reached the central part of the Atlantic Ocean, while the northern edge of the semi-circular front has been detached from the northwestern coast of Africa. We believe this detachment could be a result of the shallow layer of marine air arriving from north along the northwest coast of Africa [*Tucker and Barry,* 1984] and intruding below the dust containing air originating from the Sahara.

On April 12-13 (Plate 1f,g) the warm front of a cyclone situated over southern Europe sweeps over the region south of the Gulf of Sirte and transports dust to the Central and Eastern Mediterranean, while the transport to the subtropical Atlantic from the earlier, western Sahara source region appears to have been significantly reduced in comparison to early April. On the other hand, a continuous stream of dust from the sub-Saharan (Sahel) region of Africa appears to be transported to the Atlantic region throughout the studied month of April. This relatively steady pattern of transport could be related to the anthropogenic sources in the Sahel region studied by *Tegen and Fung* [1995], rather than the natural (desert) sources (Figure 1) included in our model study. This feature could be related to the 'Middle-Level Easterly Jet' located near the southern boundary of the dust containing 'Saharan Air Layer' moving west from Africa as described by *Karyampudi et al,* [1999]. The easterly jet occurring near the frontal area of the dust plume after being lifted up into the 'Saharan Air Layer' would indeed be consistent with the density contrast expected near the dust front.

There is striking correspondence between the observations and the model results concerning the crescent shaped patch of dust spreading into the Atlantic Ocean from sources in western Sahara (Figure 6a, Plate 2), and the dust patches over land as revealed by IDDI (Plate 1a-e) and the model generated source areas (Figures 4a-c). The filament-like shape of the dust plume detached from northwest Africa and therefore appearing to be issuing from the sub-Saharan/Sahel region has been puzzling researchers in the past (see *Mbourou et al.,* [1997] and *Husar et al.,* [1997] for a discussion). The aerosol measurements based on the Nimbus 7/TOMS satellite data confirm that moderate to high dust concentrations occur most frequently in the western Sahara desert and in an area extending west into the subtropical Atlantic Ocean *Herman et al.,* [1997]. Recent studies based on analysis of lidar data have definitively shown the maximum values of AOD for the dust plume to be located in western Sahara, west of the Ahaggar Massif in southern Algeria, and surprisingly farther north over land than

the latitude at which it apparently spreads into eastern Atlantic *Karyampudi et al.*, [1999]. This is consistent with the above results.

Around April 15 a renewed cyclogenesis near Atlas mountains takes place, and on April 16 (Plate 1h) this cyclone once again moves north, transporting dust under the clouds. On the 17th the storm moves to the Balkans. Yellow rain was reported in Belgrade on the night of 15-16 April, which was clearly associated with African cyclogenesis affecting the Balkans by *Vukmirovic et al.*, 1995.

The model results show Sahara dust sources (increased surface fluxes) on 3-5 April (Figures 4a-c) very similar to the areas indicated by IDDI over land in Plate 1a-d. Increased surface fluxes are generated in regions of increased wind stress, and a result of the increased surface winds. The source which is initially in the western Sahara on April 3 and 4 (Figures 4a,b) is related to the increased surface wind stress resulting from subsidence of air over Africa. A different source, namely resulting from the increased winds of the cyclone east of the Atlas Mountains starts to be active on April 4. On April 5, the first source region dies away, and the cyclonic center in the Gulf of Sirte becomes more active (Figure 4c). The friction velocity u_* generated by the model on April 4 (Figure 5) indicates that the surface shear stress is increased in the regions of increased fluxes (Figure 4b). A review of similar fields during a full daily cycle reveals that the surface stresses, and hence the fluxes of dust from the land surface to the atmosphere, increase during the less stable daytime boundary layer conditions, and reach a peak in the afternoon hours.

Separate sources of dust activated by subsidence and cyclone generated winds during April 3-6 create an exceptional pattern of dust transport, with one part of the dust cloud moving across the Atlantic with the anticyclonic flow, and the other part transferred north towards the Eastern Mediterranean and Balkans by a cyclonic depression. The dust spreads to the adjoining regions from a temporally changing source region. The model generated dust load on April 6 is shown in Figure 6a. While the combined Meteosat derived dust image on the same day in Plate 1d shows dust hidden under clouds of a cyclone in the Eastern Mediterranean, the extent of dust is not clear because of poor resolution based on nominal pixel size 30 km. The NOAA AVHRR visible image (Figure 6b) with finer nominal resolution of about 1km on the same day shows a better defined, shallow, dust cloud exiting from Egypt and being partially trapped by mountain ranges around the Levantine coast. The same cloud is observed to be partially overtopping the Anatolian topography to reach into the Black Sea (visible on larger area AVHRR coverage but not shown here). On the next day, AVHRR images and the model results show a marked decrease in the airborne dust (not shown) as a result of dry deposition. Although not directly comparable with dust load, further verification of increased dust

concentration at the land surface, corresponding to patches moving into the Atlantic Ocean and the Eastern Mediterranean Sea respectively, is provided by the distribution of extinction coefficient derived from visibility observations (Figure 6c). Both in the eastern part of the Levantine Basin and along the Atlantic coasts of Africa, the extinction coefficient increases during the passage of the dust cloud.

The dust transport from Africa towards the Balkan peninsula, observed to occur for a second time on April 12-13 in Plate 1f,g, is reproduced by the model results in Figure 7a. Similarly, a later storm observed on April 15-16 in Plate 1h is shown to correspond to the model dust event in Figure 7b. During the latter event, wet dust deposition in the model takes place around northern Italy and Yugoslavia (Figure 7c), and was confirmed by ground measurements at Belgrade by [Vukmirovic et al., 1997].

For revealing the 3-D structure of the combined dust storm on April 5, perspective views of the horizontal winds at 1.35 km altitude, the streamlines along a vertical cross-section, and the dust isosurface 350 $\mu g/m^3$ are shown in Plate 2. The colors superimposed on the dust isosurface are propostional to vertical velocity on this surface, with red and blue corresponding to respective areas of upward and downward motion. The subsidence south of the Atlas mountains on April 4 is evident in Plate 2, where the blue 'dimple' on the dust isosurface shows downward motions resulting in the flattening of the isosurface by divergence. This is why the dust being transferred to the Atlantic Ocean has a very shallow structure, confined within the first few kilometers of the atmosphere, mainly transported above the intensified Trade Winds system. This structure of the Trade Winds, supplied by subsidence along the periphery of the North Atlantic anticyclone is well known [*Tucker and Barry,* 1984]. On the other hand, in the eastern Mediterranean, the dust put into motion by the Sirte cyclone penetrates upwards along the warm front of the storm center by convection and frontal uplifting (Plate 2). A further feature noted in Plate 2 is the simultaneous dust storms generated near the Caspian and Aral Seas, in the far northeastern corner of the model domain, where increased near-surface winds mobilize dust from local deserts.

In the subtropical Atlantic, the troposphere can generally be divided into a lower moist and an upper dry layer, the moist layer being capped by the Trade Wind inversion. The shallow Trade Wind inversion near the African coast (around 15°N) is strengthened by the effects of subsidence on the eastern side of the subtropical anticyclone, and cooling from below by the cold upwelled water along the African coast [*Riehl,* 1954]. The temperature inversion in the eastern subtropical Atlantic does not coincide with the top of the Trade Wind regime, but is usually much shallower, at about an elevation of 500 m near Africa. The thickness of the moist surface layer depends on the balance of convection

and subsidence, and sharply rises to 2-3 km in the west, characterized with *Trade Wind cumuli* formed near the Caribbean [*Byers,* 1959]. The actual structure of the marine boundary layer over a region of variable sea surface temperature can be much more complex than described above [*Bretherton et al.,* 1995; *Wang et al.,* 1999], displaying a splitting of the layer into two by an inversion that is much shallower than the main inversion, time dependence, and changes in clouds and layer fluxes.

The air and dew point temperature profiles on a tephigram at the Sal Island rawind sounding station are shown in Figure 8. The shallow Trade Wind inversion caps relatively cooler and humid air near the surface. Immediately above the inversion there is a layer with almost isentropic (potential temperature of 35-45°C) and well mixed moisture (mixing ratio 1-2 g/kg) properties, most likely to be the air mass originating from the Sahara [*Karyampudi and Carlson,* 1988; *Chiapello et al.,* 1999]. Other rawinsonde data available at Dakar and Trinidad showed increasing temperature and humidity below the Trade Wind inversion, an increasing height of the surface mixed layer, and a decreasing thickness of the dust containing layer above, from the African coast to the Caribbean region as described by *Karyampudi et al,* 1999.

To exemplify the vertical structure of the Trade Wind system off western Africa, wind and dust concentration profiles obtained from the model at Sal Island on 1200 UTC April 4, 1994 are shown in Figure 9. The wind veers to a northeasterly direction below the trade wind inversion from the generally easterly flow above it. The humid air mass is almost entirely trapped below the inversion. The dust maximum occurs at a height of about 500m, in a layer immediately above the shallow surface layer.

The model simulated instantaneous dust concentrations are compared with the available dust concentration measurements and light extinction coefficient derived from visibility observations in Figure 10.

At Barbados Islands, the model predictions were considerably lower than the measurements, although the timing of the peak period was not dramatically different. The maximum measured concentrations of 280 $\mu g/m^3$ represented an all-time high in the observation period of 30 years [*Li et al.,* 1997].

At Sal Island, the available measurements indicated dust concentrations reaching a peak of about 260 $\mu g/m^3$ on April 5, which appeared approximately at the same time, but much smaller than the model predicted maximum concentrations. Considering the shallow structure of dust close to the source region and the relatively poor resolution of the present model in the lower layers, this agreement is considered to be satisfactory. The measured peak concentrations in April 1994 are remarkably higher than the maxima observed in the months of April during the previous years of 1992 and 1993 [*Chiapello*

et al., 1995; 1997].

At the Erdemli station, the observed peak concentration of 1600 $\mu g/m^3$ on the evening of April 6 and its decrease on April 7 agrees well with the model calculated concentrations, and with the satellite observations of Figure 6.

To check if the model simulations produced similar results with the satellite observations, we compare the dust load at three selected locations in Figure 11 According to *Dulac, et al.*, [1992] the AOD derived from Meteosat can be converted to air column integrated dust load in g/m^2, by multiplying AOD with a calibration constant in the range of 1.3-1.5. We have used a factor of 1.4 and plotted model derived and Meteosat derived dust load together. The Mediterranean is mostly cloud covered, and therefore few Meteosat data points can be obtained at Erdemli to compare with the model results. In the Atlantic region, the density front of the dust plume and the shallow transport are harder to simulate by the model. Despite these adverse factors, the timing of dust pulses and order of magnitude agreement between satellite observations and model results are considered to be satisfactory.

3.3. Teleconnections and the North Atlantic Oscillation

The rather exceptional case of blocking and jet stream interactions concurrent with the extreme dust event in April 1994 calls for an investigation of its teleconnections, such as with the North Atlantic Oscillation (NAO), as proposed by *Moulin et al.* [1997]. The time series of the seasonal NAO index for the last two decades is shown in Figure 12, where the months of March and April 1994 are observed to have relatively high NAO index values of 2.3 and 3.6 respectively. The peak index values for the positive phase NAO anomaly in Figure 12 corresponds to one of the largest 8 events in the last 20 years. The average sea level pressure pattern for the studied period indicated a dipole of low pressure near Iceland and high pressure near the Azores, typical of the large scale circulation characterized by the positive phase of NAO.

It often appears paradoxical that monthly or seasonal statistics are used to describe quasi-steady state properties of the atmosphere and to investigate dynamic processes such as the NAO. The coarse statistics hides the short-term variability and therefore appears unrelated with the day to day variability of synoptic and possibly extreme dynamic events within the period of averaging. For example, the anomalous atmospheric conditions studied above are almost undetectable in the annual NAO index for 1994. This is despite the reliable correlation of dust and NAO on an annual basis [*Moulin, et al.*, 1997], and the exceptional levels of dust concentration measured at Barbados [*Li, et al.*, 1996] and Erdemli corresponding to extreme blocking conditions (Figures 2 and 3) typical of NAO. It is not surprising

to find poor statistical correlation between transport and large scale circulation based on long term averages. Seen from this point of view, large scale atmospheric control is not readily inferred from coarse statistics unless studied carefully at the relevant time scales.

4. Conclusions

We have demonstrated a genuine Mediterranean case of meridional circulation and jet interaction resulting from Atlantic blocking, an extreme event that produced the massive cloud of Sahara dust in April 1994. The interaction of the two jets, shown here, has been suggested (*e.g. Reiter,* [1975]), but, at least to the authors' knowledge, not adequately demonstrated as a principal mechanism of Mediterranean cyclogenesis, although some limited examples have been provided by *Karein,* [1979]. The Mediterranean / North African region is considered as one of the three global areas where active cyclogenesis could be driven by jet interactions, the first two relatively stronger centers being downstream of the Rocky and Himalaya mountain ranges, where the two jet streams, typically represented by a three-wave global pattern, come into contact [*Reiter,* 1975, *Özsoy,* 1981]. In the case of the Mediterranean, meridional flow and jet interactions are expected east of a blocking high pressure system in the Atlantic, occasionally taking the form of an 'Omega High' near Spain. This type of circulation often characterizes northwesterly Mistral winds across the gap between the Pyrenees and Alps, in some cases associated with Genoa cyclogenesis, and largely influencing the Western and south Central Mediterranean with cold, dry air resulting from subsidence [*Reiter,* 1975; *Brody and Nestor,* 1980].

The maximum concentration of dust measured in April 1994 at the Barbados Island represented an extreme event possibly carrying the signatures of a large amplitude climatic fluctuation. We emphasize the role of large scale atmospheric control in creating the dust event, and show that the sequence of events leading from a strong case of atmospheric blocking, to undulations of the polar jet, its interactions and exchange of mass and energy with the subtropical jet, cyclogenesis driven by barotropic / baroclinic instabilities, subsidence and strengthening of Trade Winds, *etc.*, make up the ingredients of the studied dust transport event. We also find that this kind of hemispherical weather is associated with a prominent example for the NAO transient, and hence strengthen the earlier attempts to correlate dust transport with characteristic teleconnection patterns; however we do that on an event basis, rather than using statistical analyses on annual to seasonal time scales as considered in earlier literature.

One of the successes of our model simulations is the long range transport of dust. Simulated

dust conditions at sites distant from the source regions agree well with the observations, even under adverse conditions of subsidence and shallow boundary layer structures present in the Atlantic region. Available ground measurements and satellite data confirm the modeling results and analyses in a large area of the hemisphere. The incursion of the jet circulation into Africa creates surface suspensions of dust propagating simultaneously but in two different directions into the Atlantic and Mediterranean regions. The two pulses are dissimilar in their characteristics representing different meteorological conditions, and mesoscale characteristics; yet they are successfully simulated by the model, with an order of magnitude agreement between model results and observations. Dust reaching the Barbados Islands is underestimated, as a result of specific planetary boundary layer processes of the Trade Wind and the Trade inversion regimes not fully resolved and inadequately calibrated in the present model. These results also imply that an appropriate representation of dust size classification would be required in the model for better simulation of the long range transport.

Acknowledgments.

Modeling was performed at the Institute of Marine Sciences of the Middle East Technical University (IMS-METU) with support from the NATO TU-REMOSENS Project, thanks to Cemal Saydam of METU. AVHRR satellite data for dust events were collected at the IMS-METU, with support from the NATO SfS Project TU-BLACK SEA. Measurements of dust at Erdemli were obtained within research projects of the Turkish Scientific and Technical Research Council (TÜBİTAK) project DEBAG-79/G and METU Research Fund project AFP-98-06-01-01. Another TÜBİTAK project YDABÇAG-615/G motivated and helped production of this paper. Barbados dust measurements obtained as a part of the AEROCE program kindly have been supplied by Joe Prospero (University of Miami). Ground truth measurements at Sal Island were supplied by L. Gomes of the Université de Paris, France. Extinction coefficients retrieved from WMO visibility measurements were provided by J. Husar and R. Husar, Center for Air Pollution and Trend Analysis, Washington University.

References

Alpert, P., and B. Ziv, The Sharav cyclone: observations and some theoretical considerations, *J. Geophys. Res., 94,* 18495-18515, 1989.

Alpert, P., and E. Ganor, A jet stream associated heavy dust storm in the western Mediterranean, *J. Geophys. Res., 98,* 7339-7349, 1993.

Alpert, P., Y. J. Kaufman, Y. Shay-El, D. Tanre, A. da Silva, S. Schubert and J. H. Joseph, *Nature, 395,* 367-370, 1998.

Andreae, M. O., Raising dust in the greenhouse, *Nature, 380,* 389-390, 1996.

Avila, A. and J. Peñuelas, Increasing frequency of Saharan rains over northeastern Spain and its ecological consequences, *The Science of the Total Environment, 228,* 153-156, 1999.

Bretherton, C. S., P. Austin and D. T. Siems, Cloudiness and marine boundary layer dynamics in the ASTEX Lagrangian Experiments. Part II: Cloudiness, Drizzle, Surface Fluxes, and Entrainment, *J. Atm. Sci, 52,* 2724-2735, 1995.

Brody, L. R. and M. J. R. Nestor. Regional Forecasting Aids for the Mediterranean Basin, Handbook for Forecasters in the Mediterranean, Part 2, Naval Environmental Prediction Research Facility, Monterey, California, Technical Report TR 80-10, 178pp, 1980.

Byers, H. R. *General Meteorology,* McGraw-Hill, New York, 1959.

Chamberlain, A. C. Roughness length of sea, sand and snow. *Boundary-Layer Meteor., 25,* 405-409, 1986.

Chiapello, I., G. Bergametti, L. Gomes, B. Chatenet, F. Dulac, J. Pimenta and E. Santos Suares, An additional low layer transport of Sahelian and Saharan dust over the north-eastern tropical Atlantic, *Geophys. Res. Lett., 22,* 3191-3194, 1995.

Chiapello I., G. Bergametti, B. Chatenet, P. Bousquet, F.Dulac and E. Santos Soares, Origins of African dust transported over the northeastern tropical Atlantic, *J. Geophys. Res., 102,* 13701-13709, 1997.

Chiapello I., G. Bergametti, B. Chatenet, F.Dulac, I. Jankowiak, C. Liousse and E. Santos Soares, Contribution of the different aerosol species to the aerosol mass load and optical depth over the northeastern tropical Atlantic, *J. Geophys. Res., 104,* 4025-4035, 1999.

Danielsen, E. F., The relationship between severe weather, major dust Storms and rapid cyclogenesis, in *Synoptic Extratropical Weather Systems* edited by M. Shapiro, pp. 215-241, National Center for Atmospheric Research, NCAR, Boulder, Colo., 1974.

Dentener, F. J., G. R. Carmichael, Y. Zhang, J. Lelieveld and P. J. Crutzen, Role of mineral aerosol as a reactive surface in the global troposphere, *J. Geophys. Res., 101,* 22,869-22,889, 1996.

Duce, *et al.*, The atmospheric input of trace species to the world ocean, *Global Biogeochem. Cycles, 5,* 193-256, 1991.

Dulac, F., D. Tanre, G. Bergametti, P. Buat-Menard, M. Desbois and D. Sutton, Assessment of the African airborne dust mass over the Mediterranean Sea using Meteosat data, *J. Geophys. Res., 97,* 2489-2506,

1992.

Egger, J., P. Alpert, A. Tafferner and B. Ziv, Numerical experiments on the genesis of Sharav cyclones: idealized simulations, *Tellus, 47A,* 162-174.

El-Tantawy, A. E.-H. I., The role of the jet stream in the formation Of desert depressions in the Middle East, WMO Tech. Note 64, 159-171, World Meteorol. Organ., Geneva, Switzerland, 1961.

Flierl, G. R., V. D. Larichev, J. C. McWilliams and G. Reznik, The dynamics of baroclinic and barotropic solitary eddies, *Dyn. Atm. Oceans, 5,* 1-41, 1980.

Gilman, C. and Garrett C., Heat flux parameterizations for the Mediterranean Sea: The role of atmospheric aerosols and constraints from the water budget, *J. Geophys. Res., 99,* 5119-5134, 1994.

Guerzoni, S., R. Chester, F. Dulac, B. Herut, M.-D. Loÿe-Pilot, C. Measures, C. Migon, E. Molinaroli, C. Moulin, P. Rossini, C. Saydam, A. Soudine, P. Ziveri, The role of atmospheric deposition in the biogeochemistry of the Mediterranean Sea, *Prog. Oceanogr., 44,* 147-190, 1999.

Herman, J. R., P. K. Bhartia, O. Torres, C. Hsu, C. Seftor and E. Celarier, Global Distribution of UV-absorbing aerosols from Nimbus 7/TOMS data, *J. Geophys. Res., 102,* 16,911-16,922, 1997.

Hurrell, J. W., Influence of variations in extratropical wintertime teleconnections on Northern Hemisphere temperatures, *Geophys. Res. Lett., 23,* 665-668, 1996.

Husar R. B., J. M. Prospero, L. L. Stowe, Characterization of tropospheric over the oceans with the NOAA advanced very high resolution radiometer optical thickness operational product, *J. Geophys. Res., 102,* 16,889-16,909, 1997.

Husar, R. B. and Husar, J. D., Global Distribution of Continental Haziness, Web URL: http://capita.wustl.edu/CAPITA/CapitaI 1998.

Janjic, Z.I., Pressure gradient force and advection scheme used for forecasting with steep and small scale topography. Contrib. Atm. Phys., 50, 186-199, 1977.

Janjic, Z. I., Non-linear advection schemes and energy cascade on semi-staggered grids, *Mon. Wea. Rev., 112,* 1234-1245, 1984.

Janjic, Z. I., The step-mountain coordinate: physical package, *Mon. Wea. Rev., 118,* 1429-1443, 1990.

Janjic, Z. I., The Step-mountain Eta Coordinate Model: Further developments of the convection, viscous sublayer and turbulence closure schemes, *Mon. Wea. Rev., 122,* 927-945, 1994.

Jankowiak, I. and D. Tanre, Satellite climatology of Saharan dust outbreaks: Method and preliminary results, *J. Climate, 5,* 646-656, 1992.

Karein, A. A., The forecasting of cyclogenesis in the Mediterranean region, Ph. D. Thesis, Univ, of Edinburgh, 159 pp., 1979.

Karyampudi, V. M. and T. N. Carlson, Analysis and numerical simulations Of the Saharan air layer and its effect on easterly wave disturbances, *Journal of the Atmospheric Science, 45,* 3102-3136, 1988.

Karyampudi, M. V., S. P. Palm, J. A. Reagen, H. Fang, W. B. Grant, R. M. Hoff, C. Moulin, H. F. Pierce, O.

Torres, E. V. Browell, S. H. Melfi, Validation of the Saharan Dust Plume Conceptual Model Using Lidar, Meteosat, and ECMWF Data, *Bulletin of the American Meteorological Society, 80*, 1045-1076, 1999.

Kubilay, N. and A. C. Saydam, Trace elements in atmospheric particulates over the eastern Mediterranean; Concentrations, sources, and temporal variability, *Atmos. Env., 29,* 2289-2300, 1995.

Kubilay, N., S. Nickovic, C. Moulin and F. Dulac, An illustration of the transport and deposition of mineral dust onto the eastern Mediterranean, *Atmos. Env., 34*, 1293-1303, 2000.

Li, X., H. Maring, D. Savoie, K. Voss and J. M. Prospero, Dominance of mineral dust in aerosol light scattering in the North Atlantic trade winds, *Nature, 380,* 416-419, 1996.

Marticorena, B. and G. Bergametti, Two-year simulations of seasonal and interannual changes of the Saharan dust emissions, *Geophys. Res. Lett., 23,* 1921-1924, 1996.

Marticorena, B., G. Bergametti, B. Aumont, Y. Callot, C. N. Doume and M. Legrand, Modeling the atmospheric dust cycle.2. Simulation of Saharan dust sources, *J. Geophys. Res., 102,* 4387-4404, 1997.

Mbourou, G. N., J. J. Bertrand and S. E. Nicholson, The diurnal and seasonal cycles of wind-borne dust over Africa north of the Equator, *J. Appl. Met., 36,* 868-882, 1997.

McWilliams, J. C., An application of equivalent modons to atmospheric blocking, *Dyn. Atm. Oceans, 5,* 43-66, 1980.

Mesinger, F., Z. I. Janjic, S. Nickovic, D. Gavrilov and D. G. Deaven, The step-mountain coordinate: model description and performance for cases of Alpine lee cyclogenesis and for a case of an Appalachian redevelopment, *Mon. Wea. Rev., 116,* 1493-1518, 1988.

Miller, R. L. and I. Tegen, Climate response to soil dust aerosols, *Journal of Climate, 11,* 3247-3267, 1998.

Miller, R. L. and I. Tegen, Radiative forcing of a tropical direct circulation by soil dust aerosols, *Journal of the Atmospheric Sciences, 56,* 2403-2433, 1999.

Moulin, C., C. E. Lambert, F. Dulac and U. Dayan, Control of atmospheric export of dust from North Africa by the North Atlantic oscillation. *Nature, 387,* 691-694, 1997.

Moulin, M. C., Transport atmospherique des poussieres africaines sur la Mediterranee et l'Atlantique: climatologie satellitale a partir des images Meteosat VIS (1983-1994) et relations avec le climat, 1997. PhD Thesis, Universite PARIS 6, France.

Nickovic, S., and S. Dobricic, A model for long-range transport of desert dust, *Mon. Wea. Rev., 124,* 2537-2544, 1996.

Nickovic, S., D. Jovic, O. Kakaliagou, and G. Kallos, Production and long-range transport of desert dust in the Mediterranean region: Eta model simulations. 22nd NATO/CCMS International Technical Meeting on Air Pollution Modelling and Its Applications, 2-6 June 1997, Clermont-Ferrand, France, 1997.

Nickovic, S., A. Papadopoulos, O. Kakaliagou and G. Kallos, Model for prediction of desert dust cycle in the atmosphere, *J. Geophys. Res.,* , *this issue*, 2000.

Ott, S. T., A. Ott, D. W. Martin, J. A. Young, Analysis of a trans-Atlantic Saharan dust Outbreak based on

satellite and GATE data, *Mon. Wea. Rev., 119,* 1832-1850, 1991.

Özsoy, E., On the Atmospheric Factors Affecting the Levantine Sea, *Tech. Rep. 25,* European Centre for Medium Range Weather Forecasts (ECMWF), Reading, England, 30 pp., 1981.

Özsoy, E., Sensitivity to Global Change in Temperate Euro-Asian Seas (the Mediterranean, Black Sea and Caspian Sea): A Review, in P. Malanotte-Rizzoli and V. N. Eremeev, (editors), *The Eastern Mediterranean as a Laboratory Basin for the Assessment of Contrasting Ecosystems*, NATO Science Series 2, Environmental Security, **51**, Kluwer Academic Publishers, Dordrecht, pp. 281-300, 1999.

Perry, K. D., T. A. Cahill, R. A. Eldred, and D. D. Dutcher, Long-range transport of North-African dust to the eastern United States. *J. Geophys. Res., 102*, 11225-11238, 1997.

Prezerakos, N. G., Synoptic flow patterns leading to the generation of north-west African depressions, *International Journal of Climatology, 10,* 33-48, 1990.

Prezerakos, N. G., S. C. Michaelides and A. S. Vlassi, Atmospheric synoptic conditions associated with the initiation of north-west African depressions, *International Journal of Climatology, 10,* 711-729, 1990.

Prezerakos, N. G., Dust storms over Sahara desert leading to dust deposit or coloured rain in the south Balkans, in *First LAS/WMO International Symposium on Sand and Dust Storms (ISSDS-I)*, Damascus, Syrian Arab Republic, 2-7 November, 1997. World Meteorological Organization, WMO/TD-No.864, pp.21-38, 1998.

Prospero, J. M. and R. T. Nees, Impact of the Norh African drought and El Niño on mineral dust in the Barbados Trade Winds, *Nature, 320,* 735-738, 1986.

Prospero, J.M., Arid regions as sources of mineral aerosols in the marine atmosphere, *Geological Societ of America, Special Paper 186,* 71-86, 1981.

Reiter, E. R. Handbook for Forecasters in the Mediterranean; Weather Phenomena of the Mediterranean Basin; Part 1: General Desciription of the Meteorological Processes, *Tech. Pap. 5-75,* 344 pp., Environmental Prediction Research Facility, Naval Postgraduate School, Monterey, California, 1979.

Riehl, H., *Tropical Meteorology,* McGraw-Hill, New York, 392 pp., 1954.

Segal, M., On the impact of thermal stability on some rough flow effects over mobile surfaces, *Boundary-Layer Meteor., 52,* 193-198, 1990.

Schollaert, S. E. and J. T. Merrill, Cooler sea surface west of the Sahara Desert correlated to dust events, *Geophys. Res. Lett., 25,* 3529-3532, 1998.

STC Technical Reports 2906 and 2959, Asian duststorms and their effects on radiation and climate, Part I and Part II. *Prepared for* National Oceanic and Atmospheric Administration. Science and Technology Corporation, Hampton, Virginia, 1995 and 1996.

Tegen I., and I. Fung, Contribution to the atmospheric mineral aerosol load from land surface modification, *J. Geophys. Res., 100,* 18707-18726, 1995.

Tegen, I., A. A. Lacis and I. Fung, The influence on climate forcing of mineral aerosols from disturbed soils,

Nature 380, 419-422, 1996.

Tucker, G. B. and R. G. Barry, Climate of the North Atlantic Ocean, in *Climates of the Oceans, World Survey of Climatology,* edited by H. Van Loon, *15*, Elsevier, 193-257, 1984.

Wallace, J. M. and M. L. Blackmon, Observations of low-frequency atmospheric variability, in *Large-Scale Dynamical Processes in the Atmosphere,* edited by B. J. Hoskins and R. P. Pearce, pp. 54-95, Academic Press, 1983.

Vukmirovic, Z., J. Marendic-Miljkovic, S. Rajsic, M. Tasic and V. Novakovic, Resuspension of Trace Metals in Belgrade under conditions of drastically reduced emission levels, *Water air and Soil Pollution*, **93**, 137-156, 1997.

Wang, Q., K. Suhre, P. Krummel, S. Siems, L. Pan, T. S. Bates, J. E. Johnson, D. H. Lenschow, B. J. Heubert, G. L. Kok, R. D. Schillawski, A. Prévot and S. Businger, Characteristics of marine boundary layers during Lagrangian Measurement Periods, 1. General Conditions and Characteristics, *J. Geophys. Res., 104,* 21,751-21,765, 1999.

Wilson, M. F., and A. Henderson-Sellers, Land cover and soils data sets for use in general circulation climate models, *J. Climatol., 5,* 119-143, 1984.

E. Özsoy, Institute of Marine Sciences, Middle East Technical University P.K. 28 Erdemli - İçel 33731 Turkey. (e-mail: ozsoy@ims.metu.edu.tr)

N. Kubilay, Institute of Marine Sciences, Middle East Technical University P.K. 28 Erdemli, İçel 33731 Turkey. (e-mail: kubilay@ims.metu.edu.tr)

S. Nickovic, Euro-Mediterranean Centre on Insular Coastal Dynamics, Foundation for International Studies, University of Malta, St. Paul Street, Valletta, Malta. (e-mail: nicko@icod.org.mt)

C. Moulin, Laboratoire des Sciences du Climat et de l'Environnement (CEA/CNRS), CE Saclay - bat.709, 91191 Gif-sur-Yvette, France. (e-mail: moulin@lsce.saclay.cea.fr)

Received _____

Figure 1. The surface topography and soil type classification showing desert and semi-desert areas used in the model.

Figure 2. Geopotential height at $500hPa$ pressure level for the northern hemisphere on (a) April 1, (b) April 5, (c) April 9, (d) April 13, (e) April 17. The source for the data is NOAA Climate Diagnostic Center (plotting page URL http://www.cdc.noaa.gov/HistData/)

Figure 3. Daily wind speed (shading) and direction (unit vectors) at $250hPa$ pressure level for the northern hemisphere, on (a) April 1, (c) April 5, (c) April 9, (d) April 13, 1994. The source for the data is NOAA Climate Diagnostic Center (plotting page URL http://www.cdc.noaa.gov/HistData/)

Figure 4. Model generated dust suspension flux ($mg\ m^{-2}h^{-1}$) at 1200 UTC on (a) April 3, (b) April 4, (5) April 5, 1994.

Figure 5. Model friction velocity $u_\star$ (m/s) on April 4, 1994, at 1200 UTC.

Figure 6. (a) Model dust load on April 6, 1200 UTC, (b) NOAA AVHRR image of dust storm on April 6, 1428 UTC and (c) light extinction coefficient derived from visibility observations on April 6, 1994.

Figure 7. Model dust load on (a) April 12, 1200 UTC and (b) April 16, 1200 UTC and (c) model wet dust deposition on April 17, 1994, 1200 UTC.

Figure 8. Tephigram from a rawidsonde profile at Sal Island on April 4 1994 1200 UTC.

Figure 9. The vertical structure of the trade wind system obtained from the model: Temperature, relative humidity (dotted line), east and north (dotted line) wind speed and dust concentration profiles at Sal Island on April 4 1994 1200 UTC.

Figure 10. Comparison of model simulated (lines) dust concentration time series with the available ground observations (points), and light extinction coefficient derived from visibility observations. (a) Barbados, (b) Sal Island, and (c) Erdemli. (For light extinction in Erdemli, the data available at the closest stations Haifa, Paphos and Iskenderun have been plotted.)

Figure 11. Model derived (grey circles) versus Meteosat AOD derived (black squares) air column integrated dust load (g/m^2) at (a) Erdemli, (b) Sal Island, and (c) at a location in the Atlantic Ocean west of Sal Island. The Meteosat derived AOD is converted to dust load as described in the text

Figure 12. Time variation of the seasonal NAO index for the last two decades. The vertical dashed line is positioned at April 1994. The horizontal dotted line marks the NAOI value of 3.6 for the same month

Plate 1. Satellite derived daily composite images of Aerosol Optical Depth (AOD) derived from Meteosat visible data over the sea and Infrared Difference Dust Index (IDDI) derived from raw counts of infrared data over land on (a) April 3, (b) April 4, (c) April 5, (d) April 6, (e) April 7, (f) April 12, (g) April 13, (h) April 16, 1994.

Plate 2. Three dimensional visualization of model results: Horizontal wind at 1.35 km elevation, the streamlines on a vertical cross-section across Europe and Africa, dust isosurface for 350 $\mu g/m^3$, with colouring based on the vertical velocity on the same isosurface on April 5 . Red/blue colours on the isosurface respectively correspond approximate levels of $\pm 0.02 m/s$ in vertical velocity.

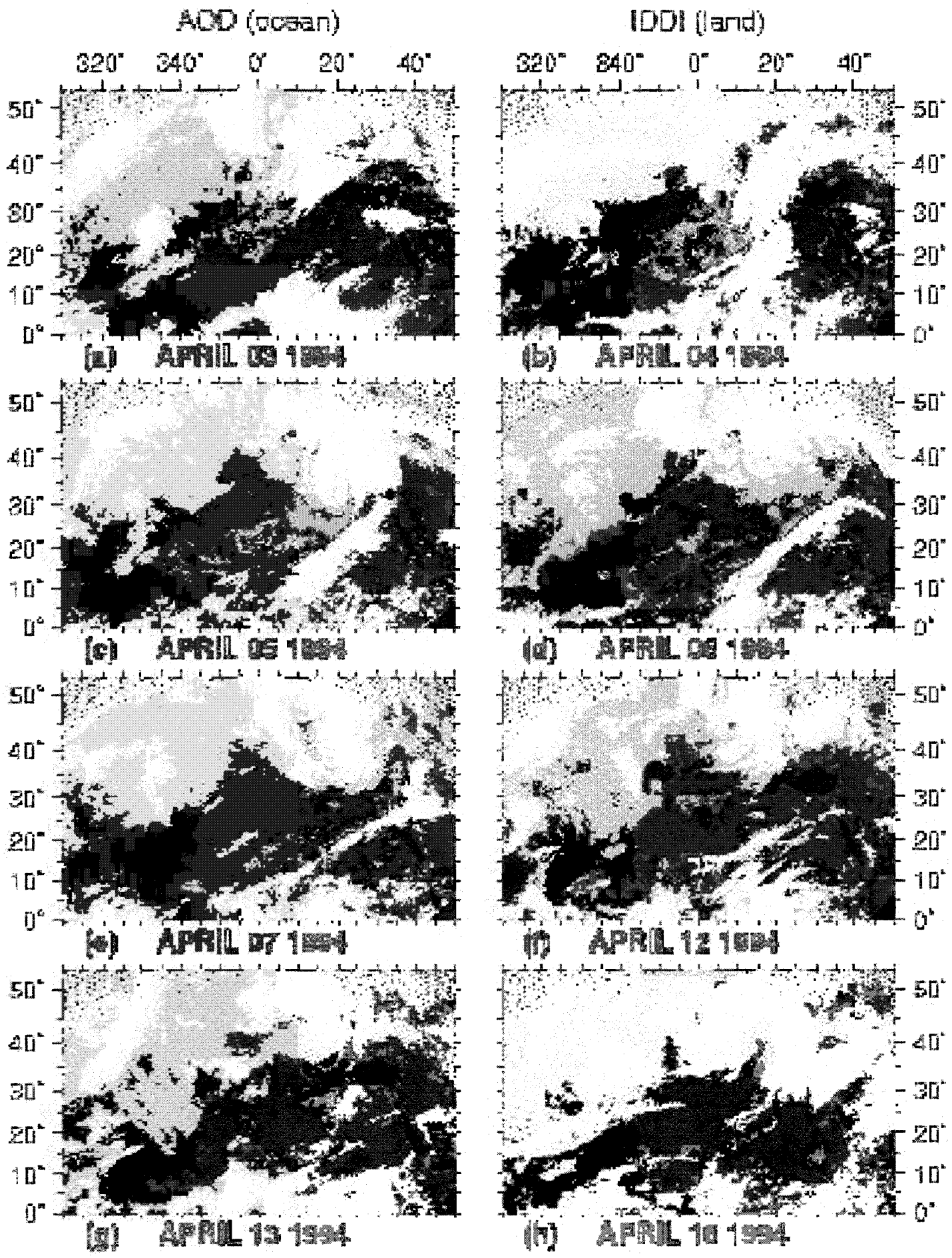
ADD (ocean)
IDDI (land)
320° 340° 0° 20° 40°
50° 40° 30° 20° 10° 0°
(a) APRIL 03 1994
(b) APRIL 04 1994
(c) APRIL 05 1994
(d) APRIL 08 1994
(e) APRIL 07 1994
(f) APRIL 12 1994
(g) APRIL 13 1994
(h) APRIL 10 1994

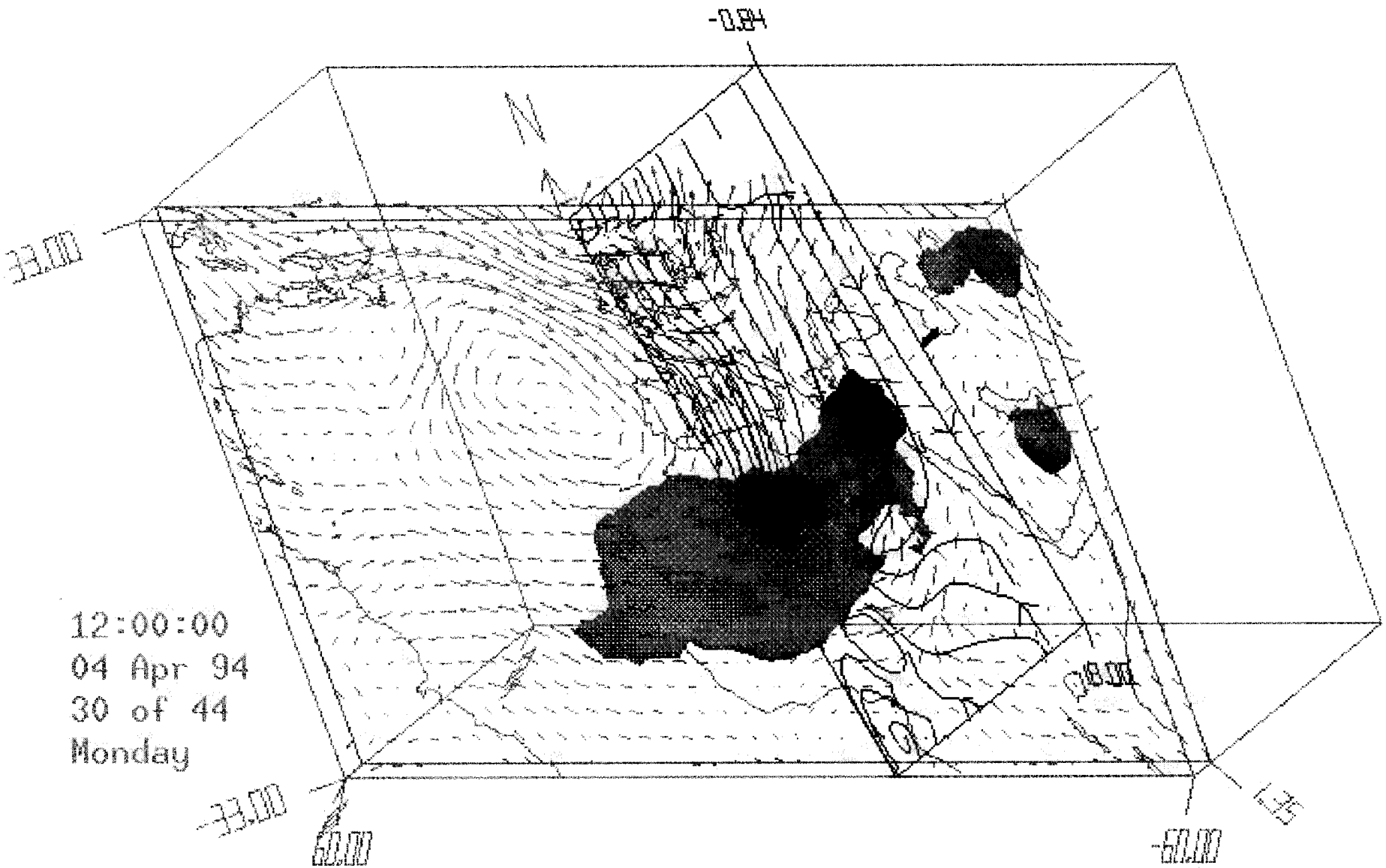
12:00:00
04 Apr 94
30 of 44
Monday

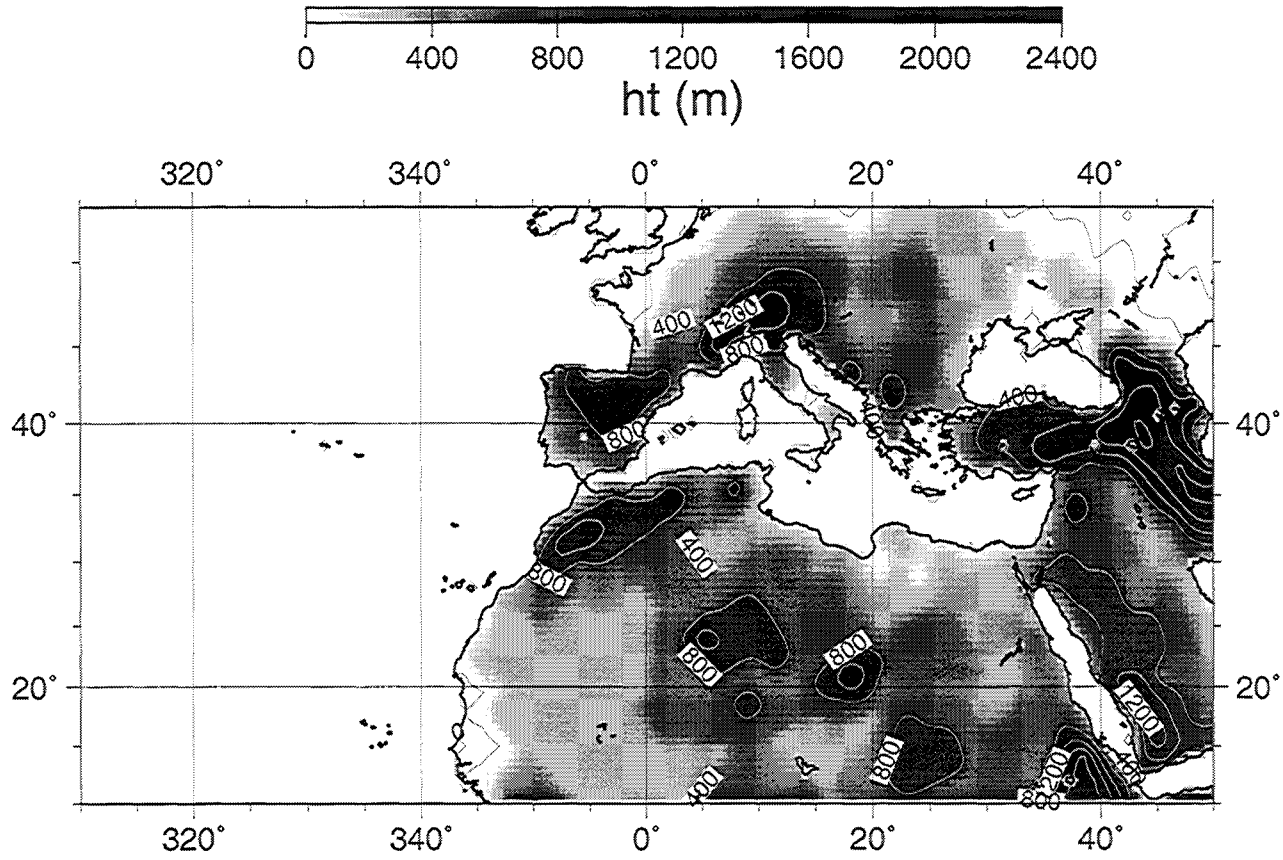
0
400
800
1200
1600
2000
2400
ht (m)
320°
340°
0°
20°
40°
40°
20°
400
1200
800
800
400
800
800
1800
1200

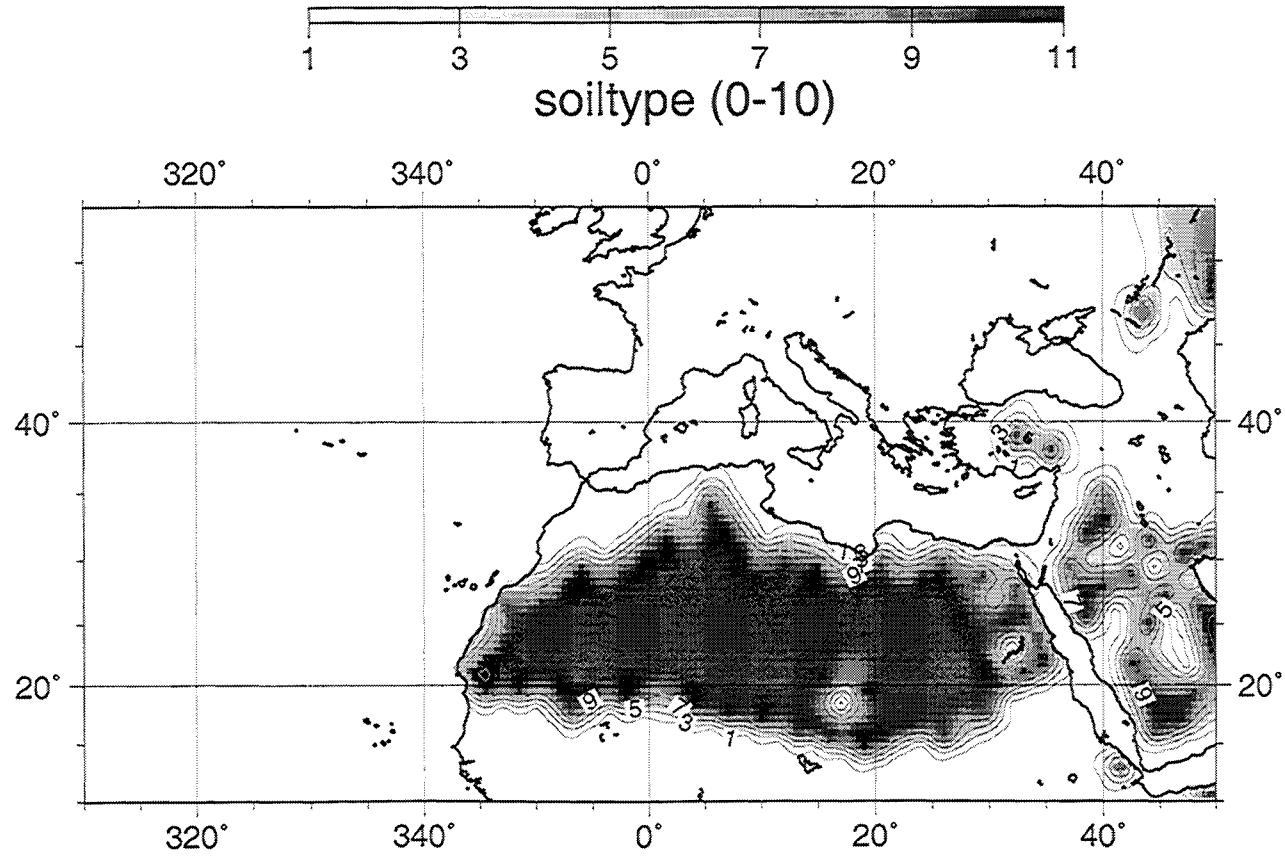
1
3
5
7
9
11
soiltype (0-10)
320°
340°
0°
20°
40°
40°
20°
9
5
7
1
9
9
5
9

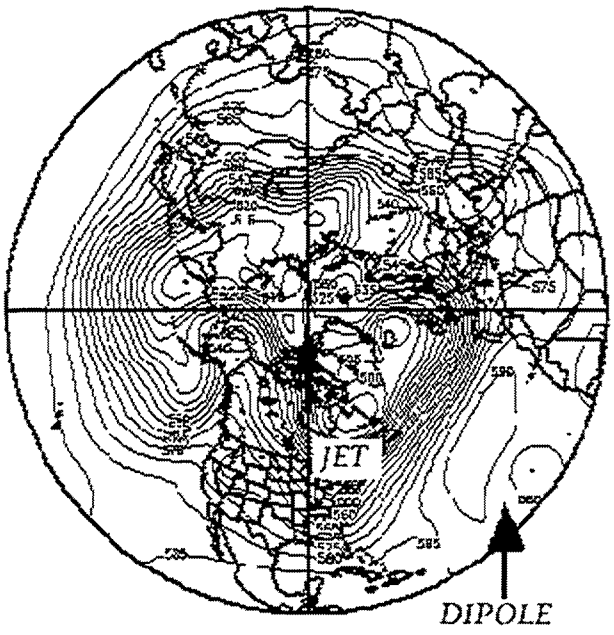
JET
DIPOLE

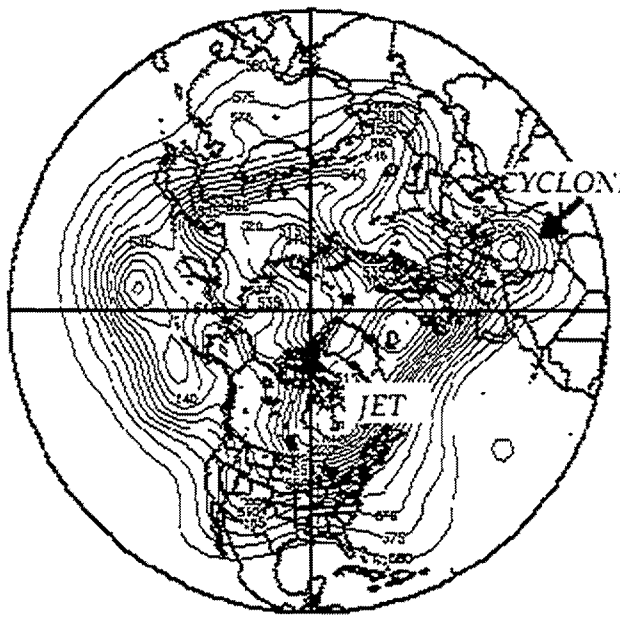
CYCLONE
JET

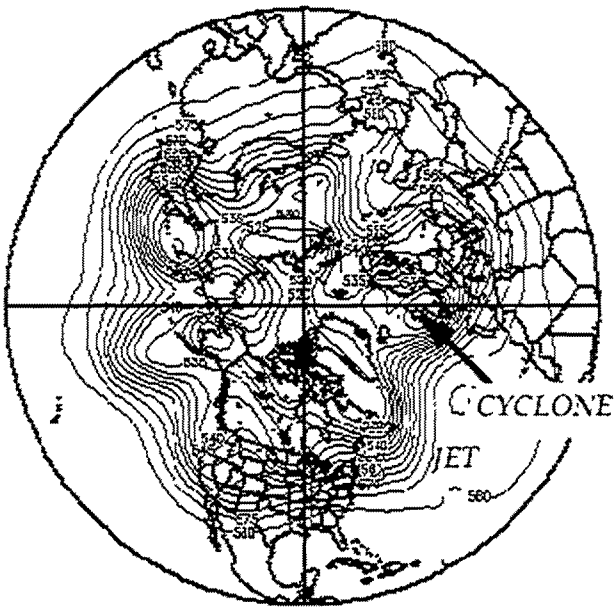
CYCLONE
JET

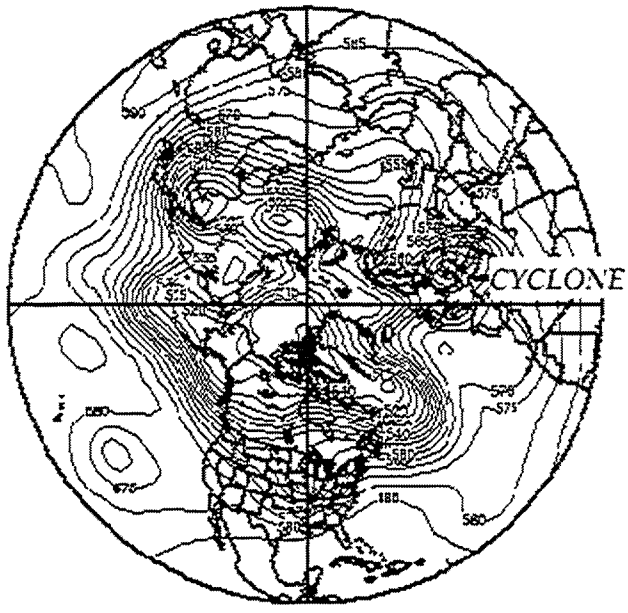
CYCLONE

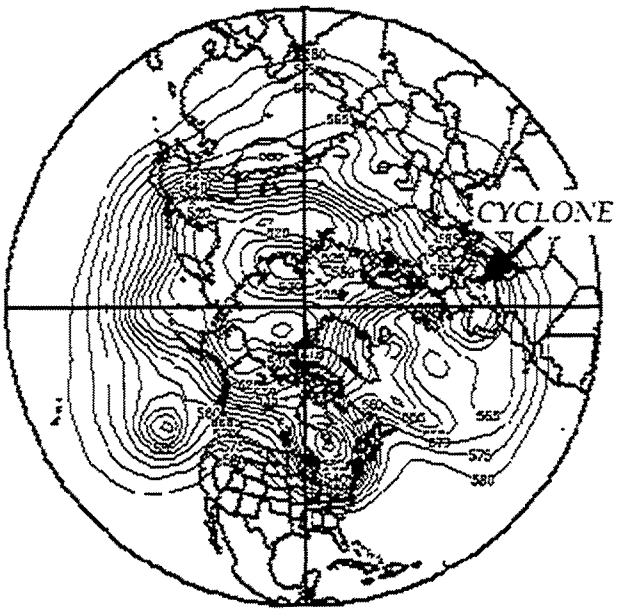
CYCLONE

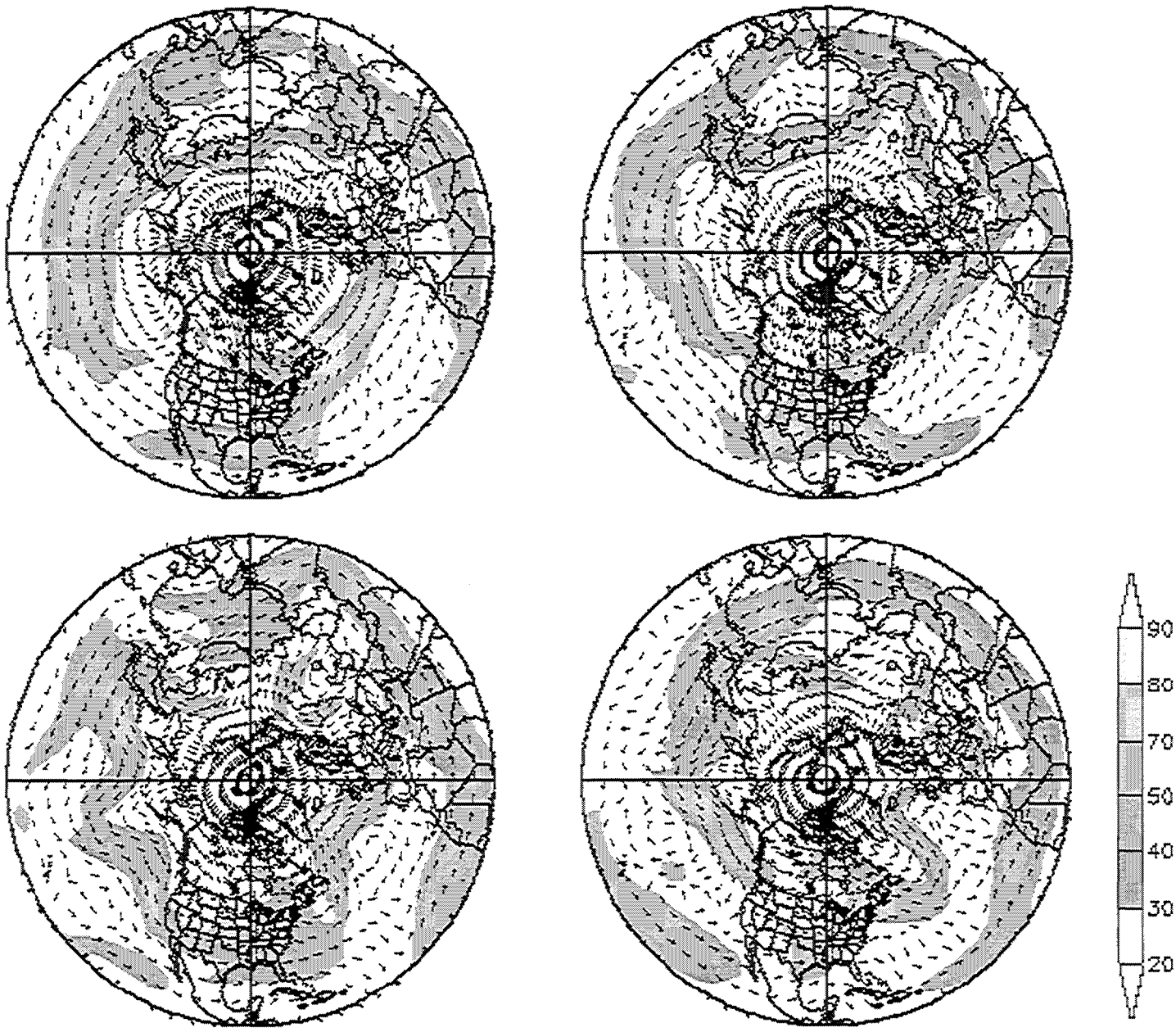
90
80
70
50
40
30
20

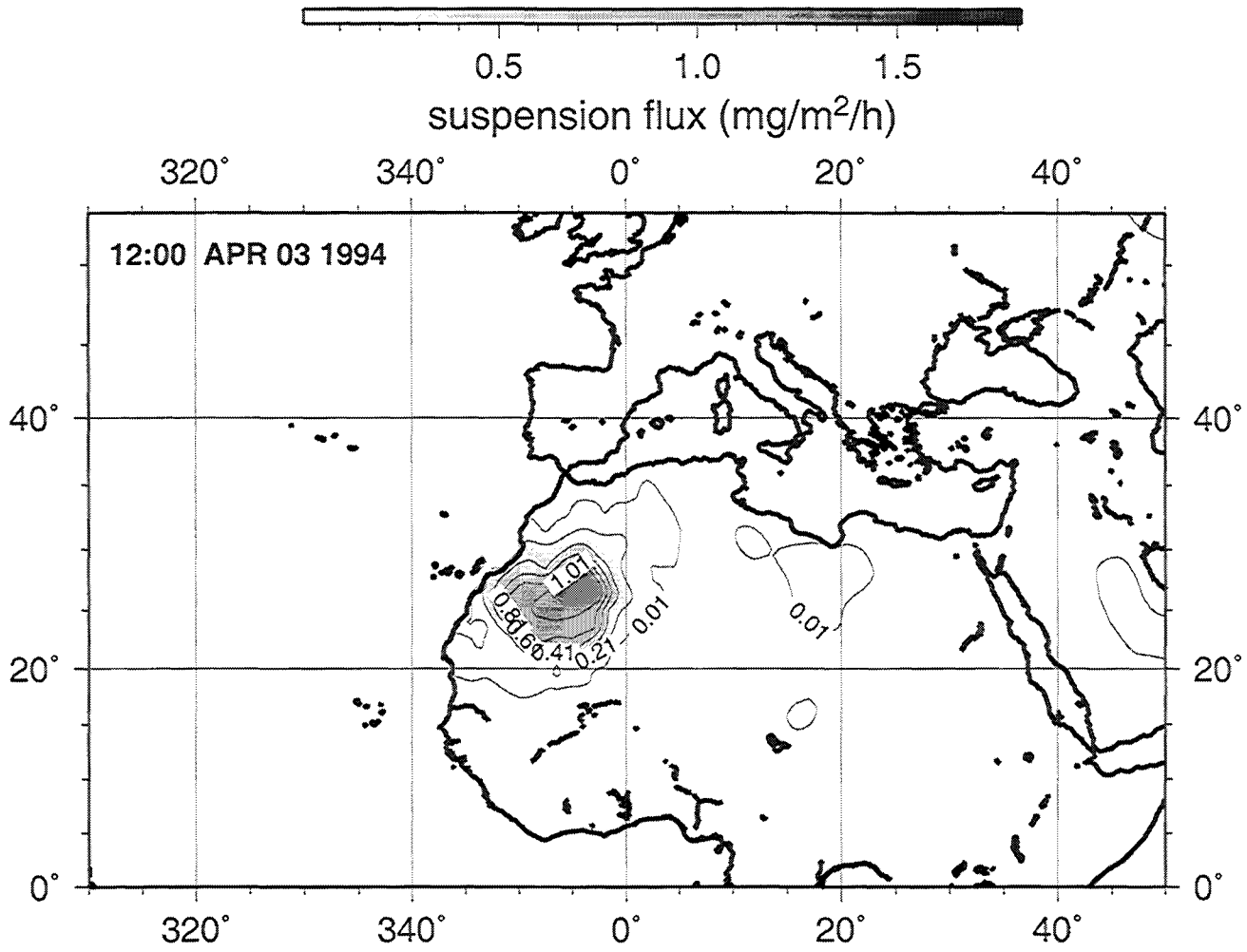
0.5
1.0
1.5
suspension flux (mg/m2/h)
320˚
340˚
0˚
20˚
40˚
12:00 APR 03 1994
40˚
20˚
0˚
1.01
0.81
0.61
0.41
0.21
0.01
0.01

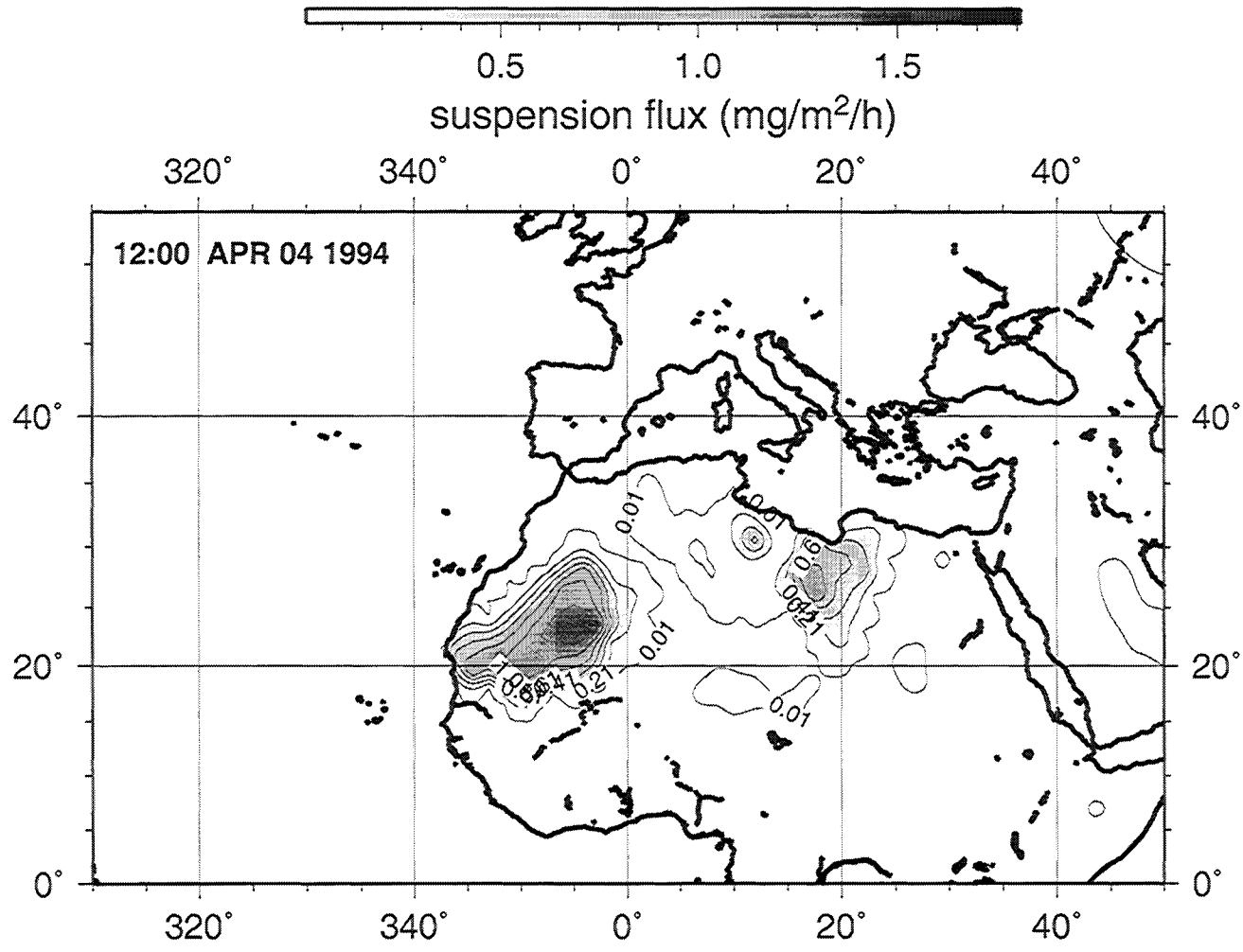
0.5
1.0
1.5
suspension flux (mg/m2/h)
320°
340°
0°
20°
40°
12:00 APR 04 1994
40°
20°
0°
0.01
0.01
0.01
0.01
0.21
0.41
0.61

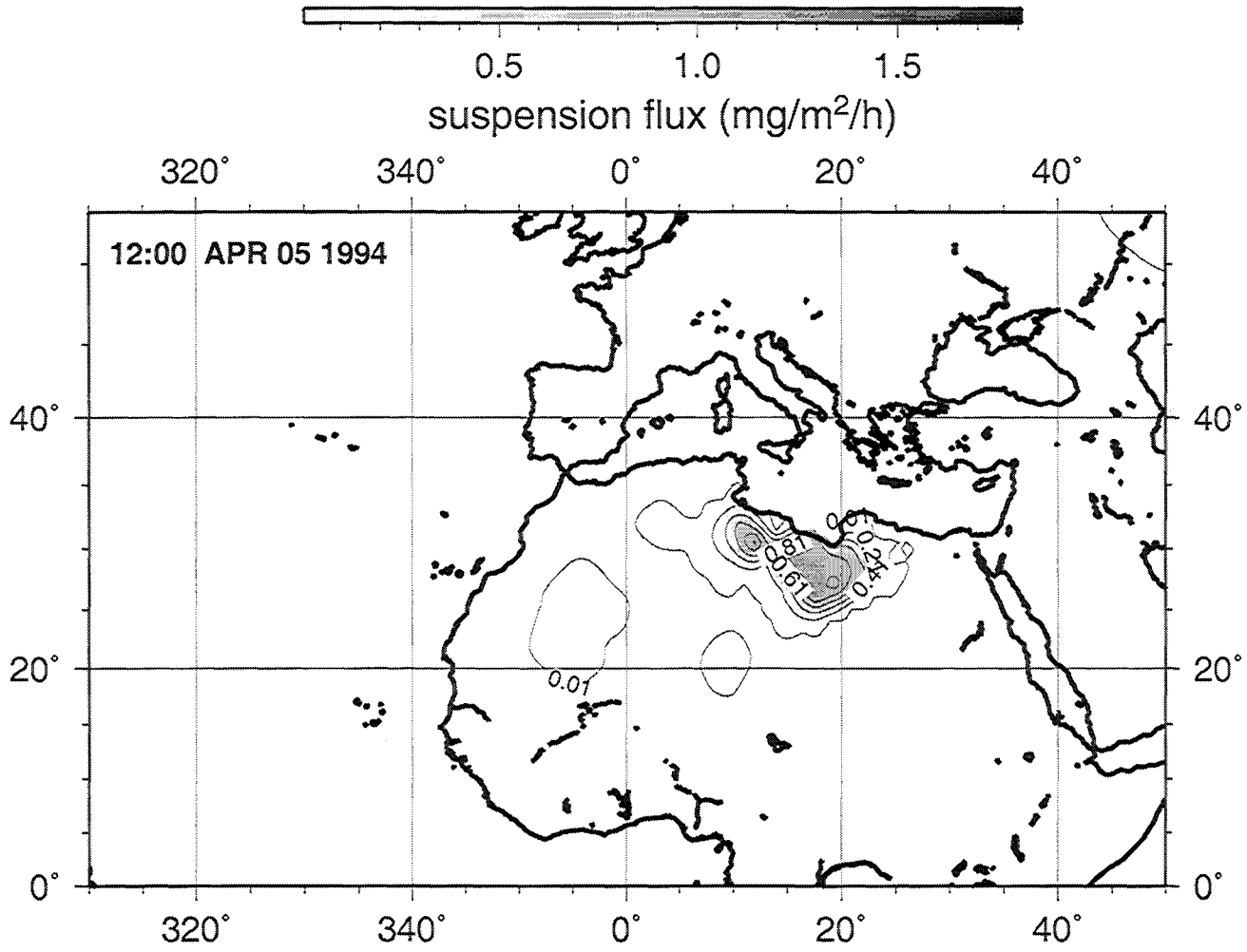
0.5
1.0
1.5
suspension flux (mg/m2/h)
320˚
340˚
0˚
20˚
40˚
12:00 APR 05 1994
40˚
20˚
0˚
0.01
0.61
0.24

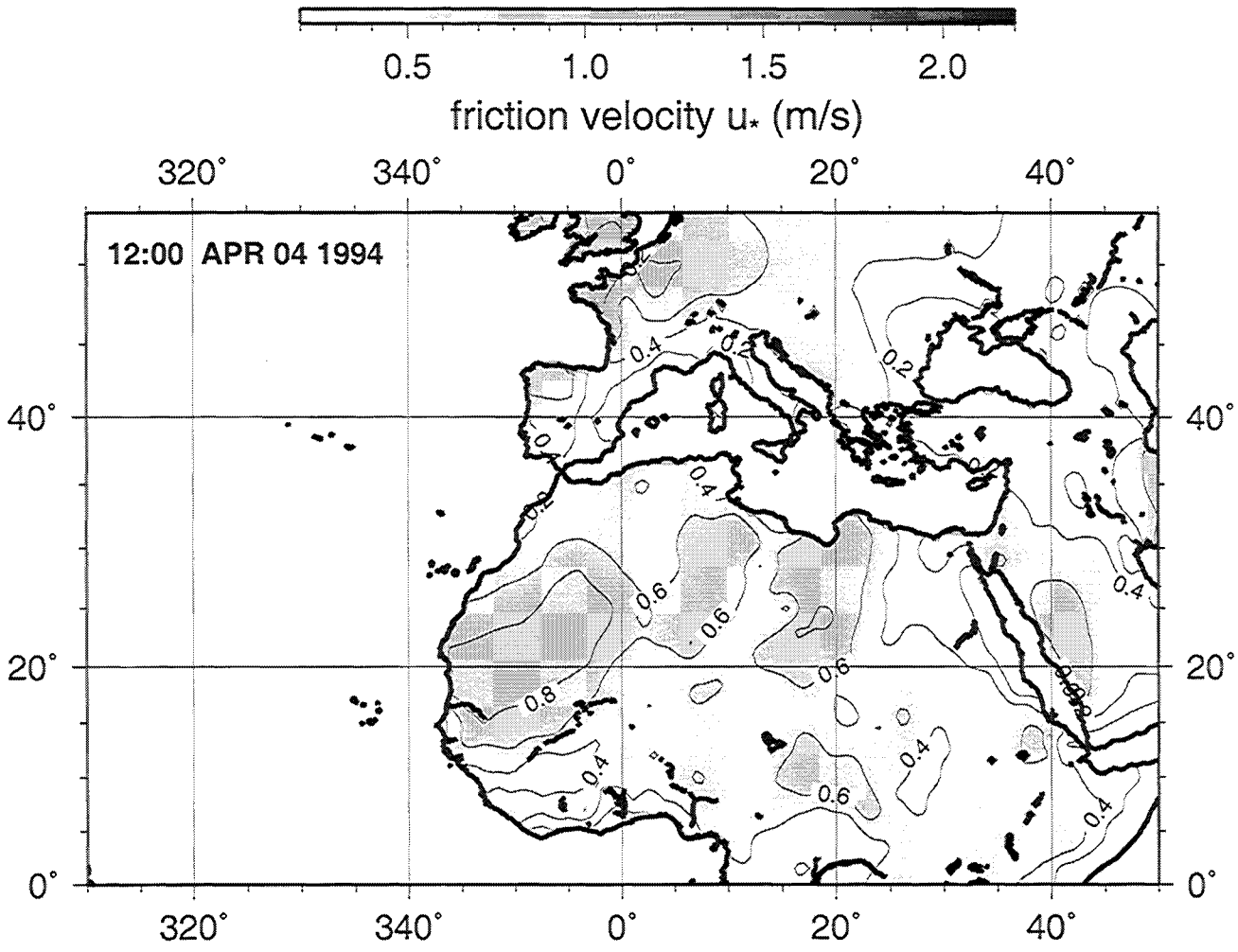
0.5
1.0
1.5
2.0
friction velocity u* (m/s)
320°
340°
0°
20°
40°
12:00 APR 04 1994
40°
20°
0°
0.2
0.4
0.6
0.8

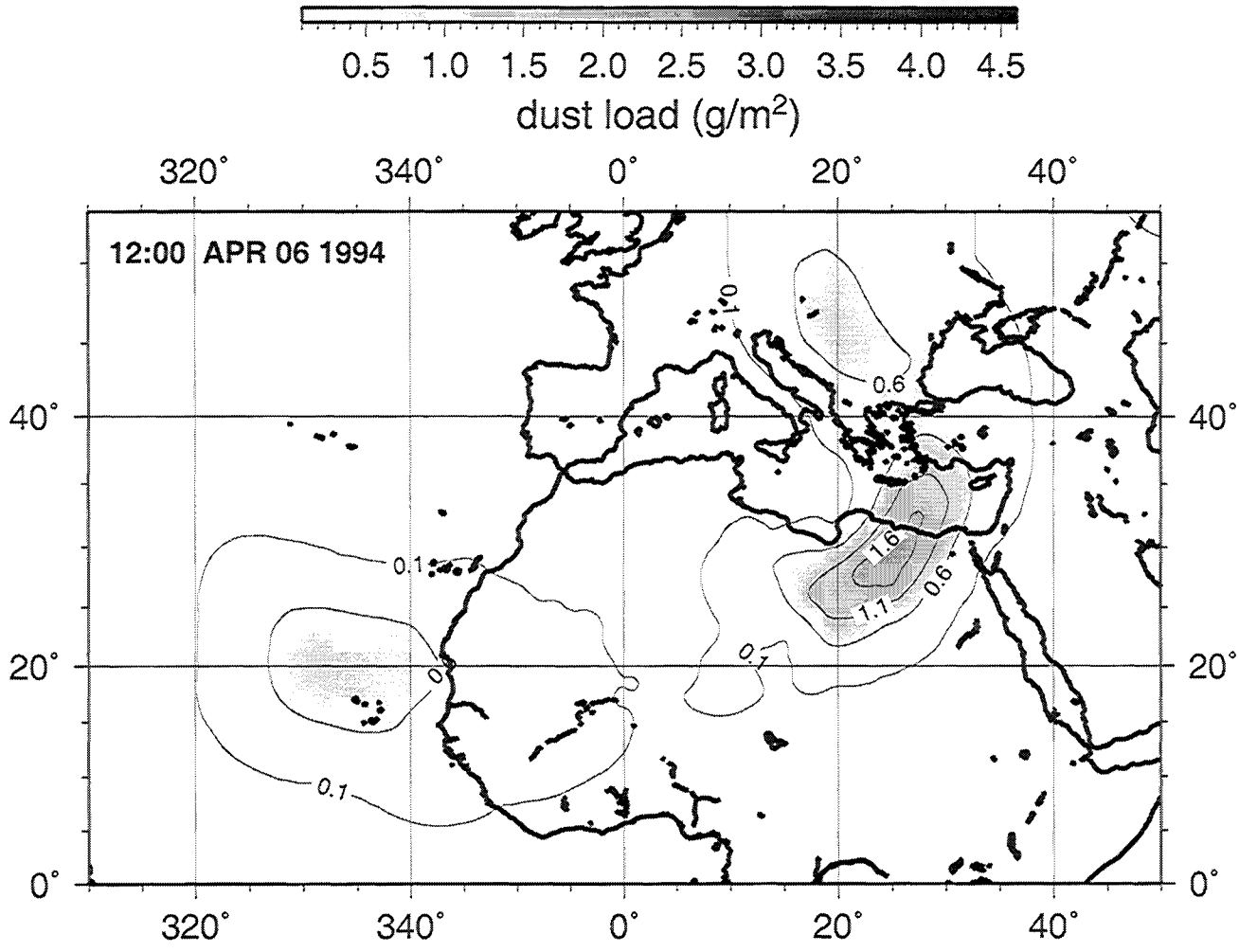
0.5 1.0 1.5 2.0 2.5 3.0 3.5 4.0 4.5
dust load (g/m2)
12:00 APR 06 1994
320°
340°
0°
20°
40°
0.1
0.6
1.6
1.1
0.7

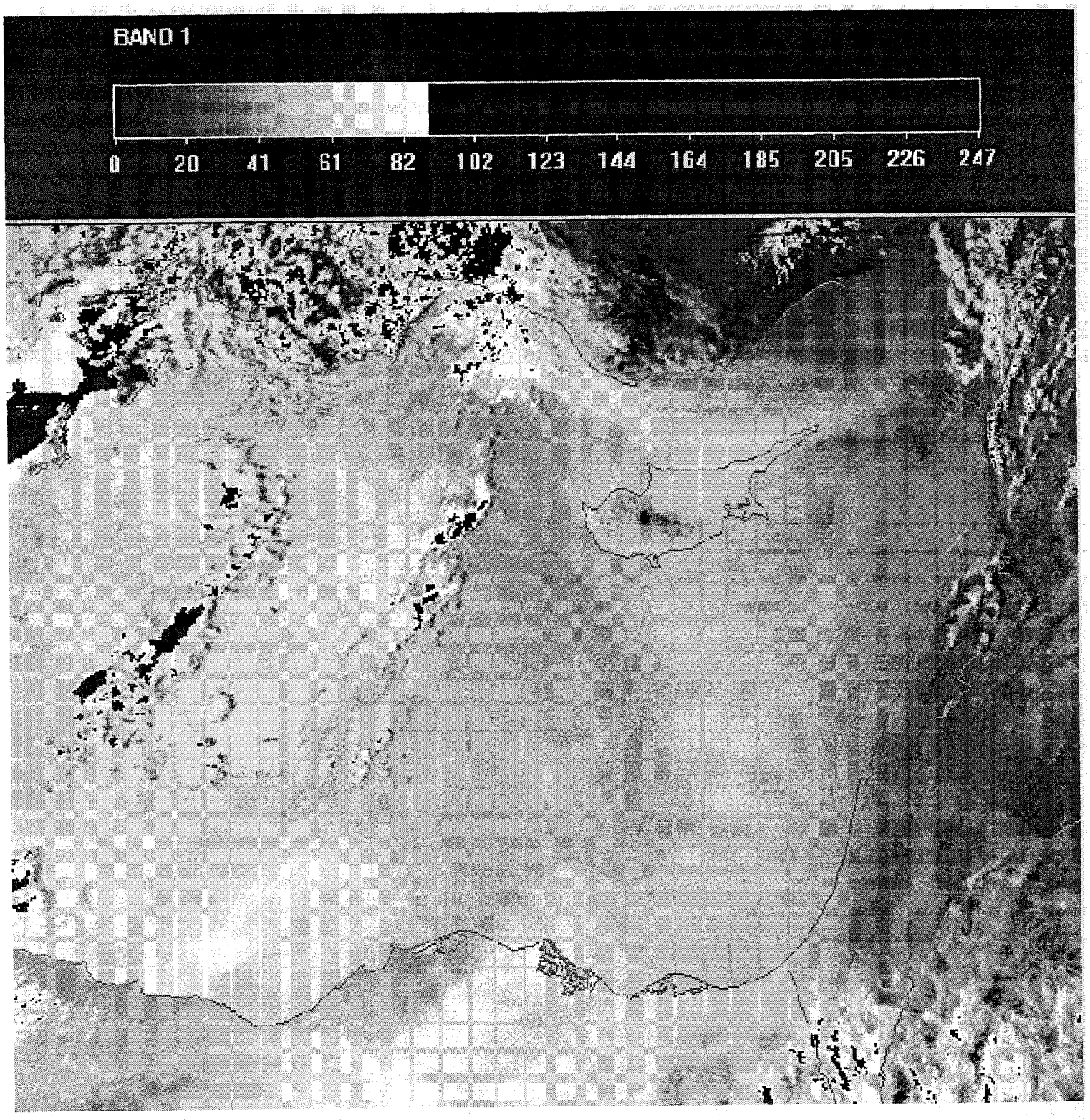
BAND 1
0
20
41
61
82
102
123
144
164
185
205
226
247

visibility extinction km^{-1} 06 April 1994

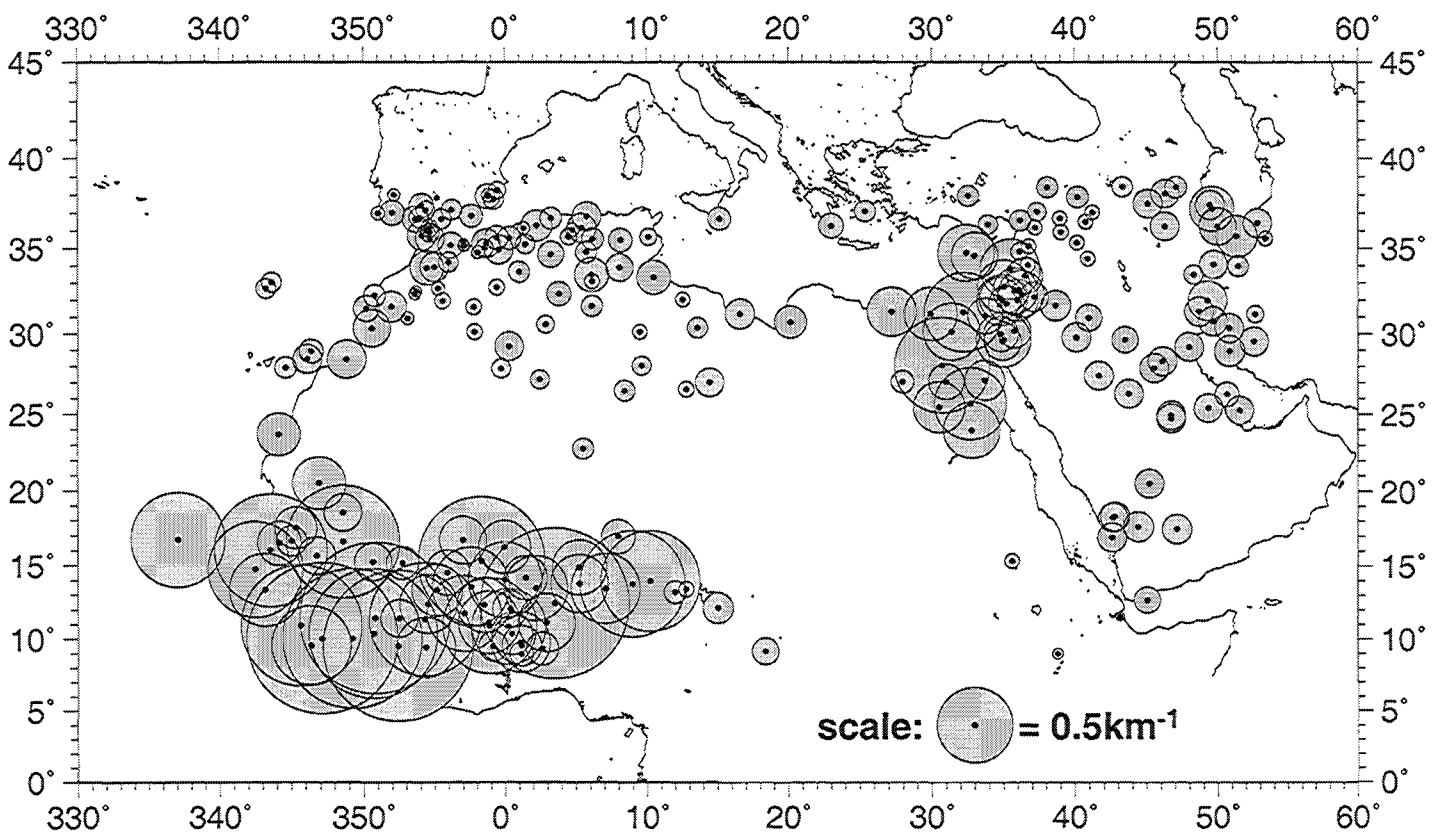

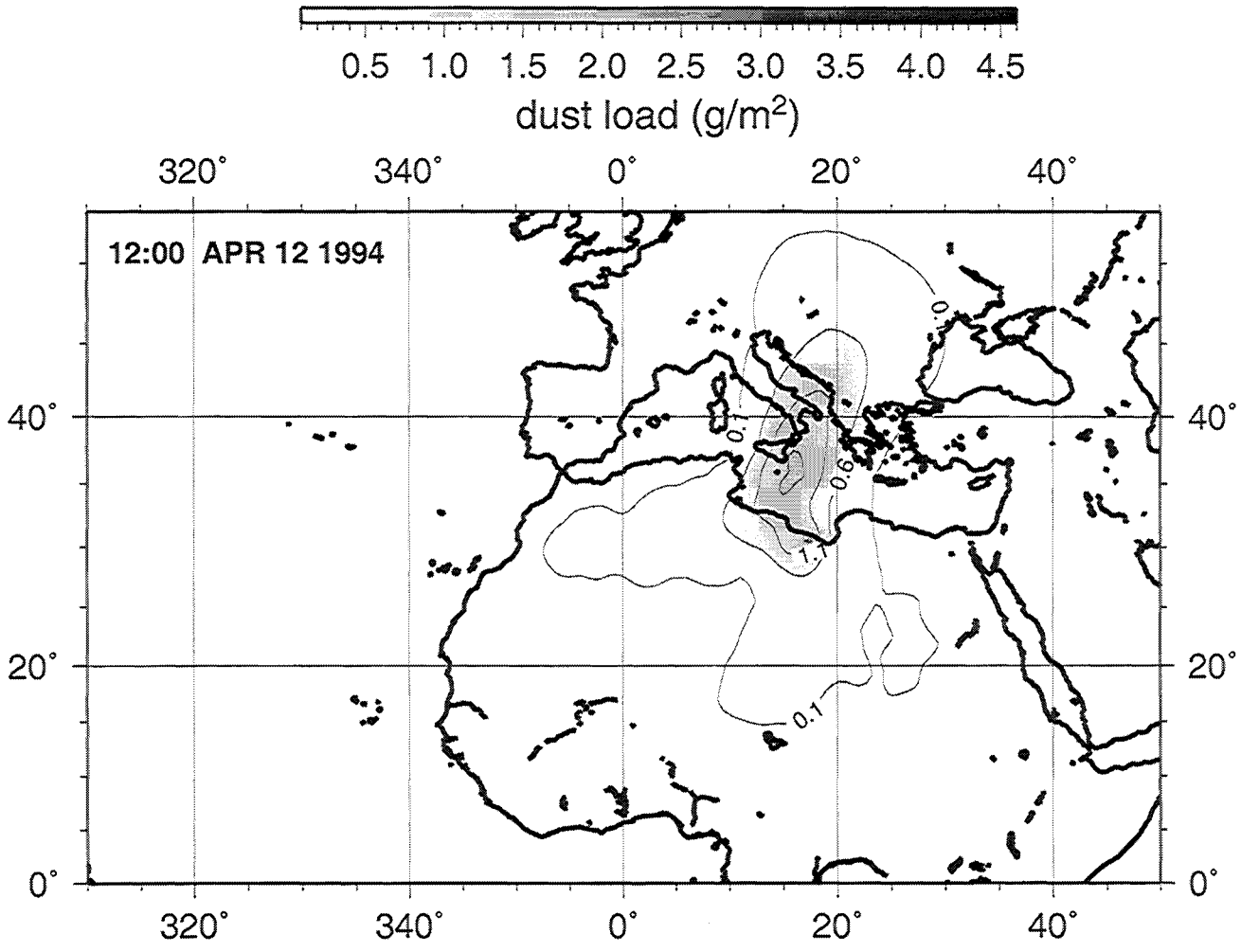
0.5 1.0 1.5 2.0 2.5 3.0 3.5 4.0 4.5
dust load (g/m2)
12:00 APR 12 1994
320°
340°
0°
20°
40°
0.1
0.6
1.1
0.1

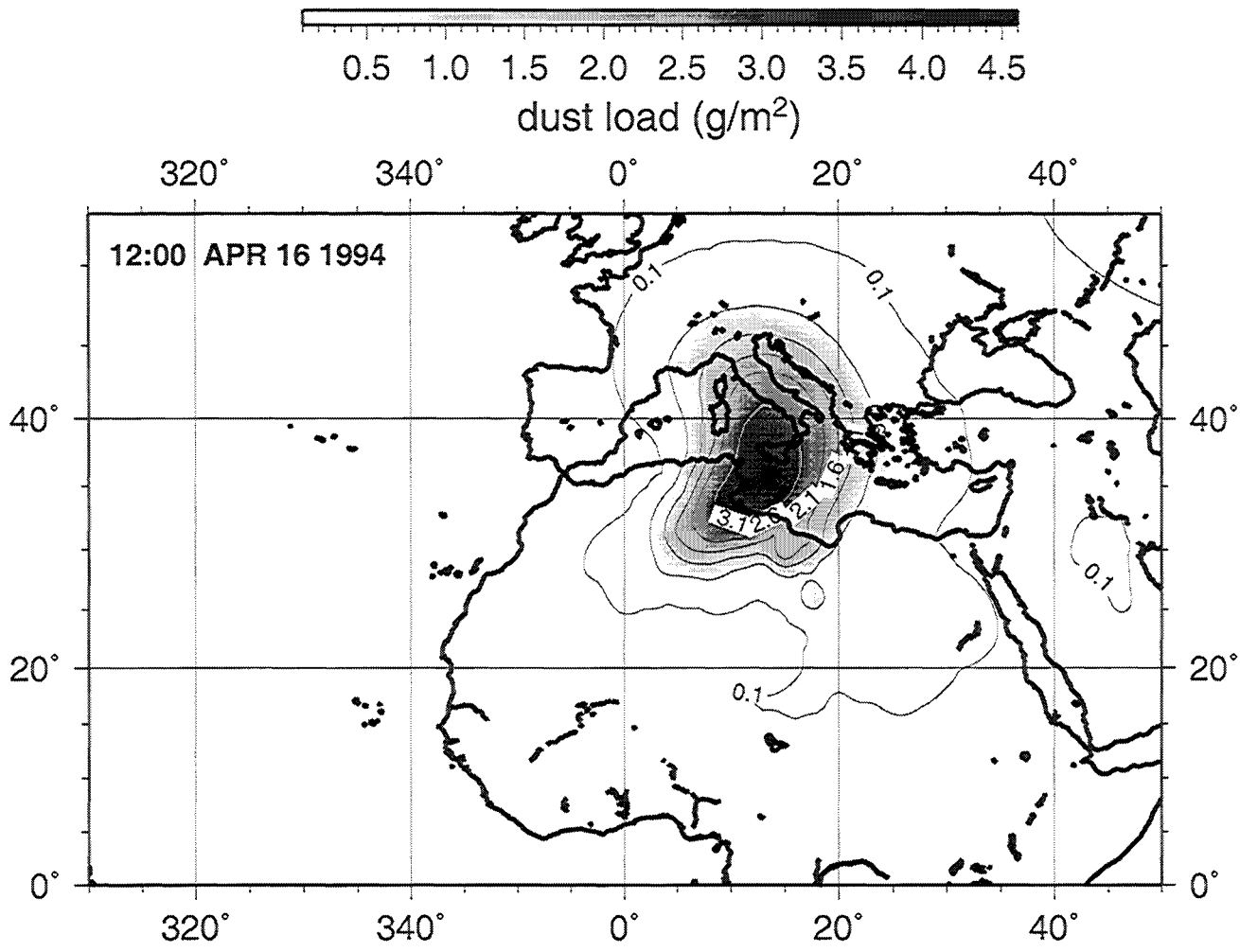
0.5 1.0 1.5 2.0 2.5 3.0 3.5 4.0 4.5
dust load (g/m2)
320° 340° 0° 20° 40°
12:00 APR 16 1994
0.1
0.1
3.1
2.1
1.6
0.1
0.1
40° 20° 0°

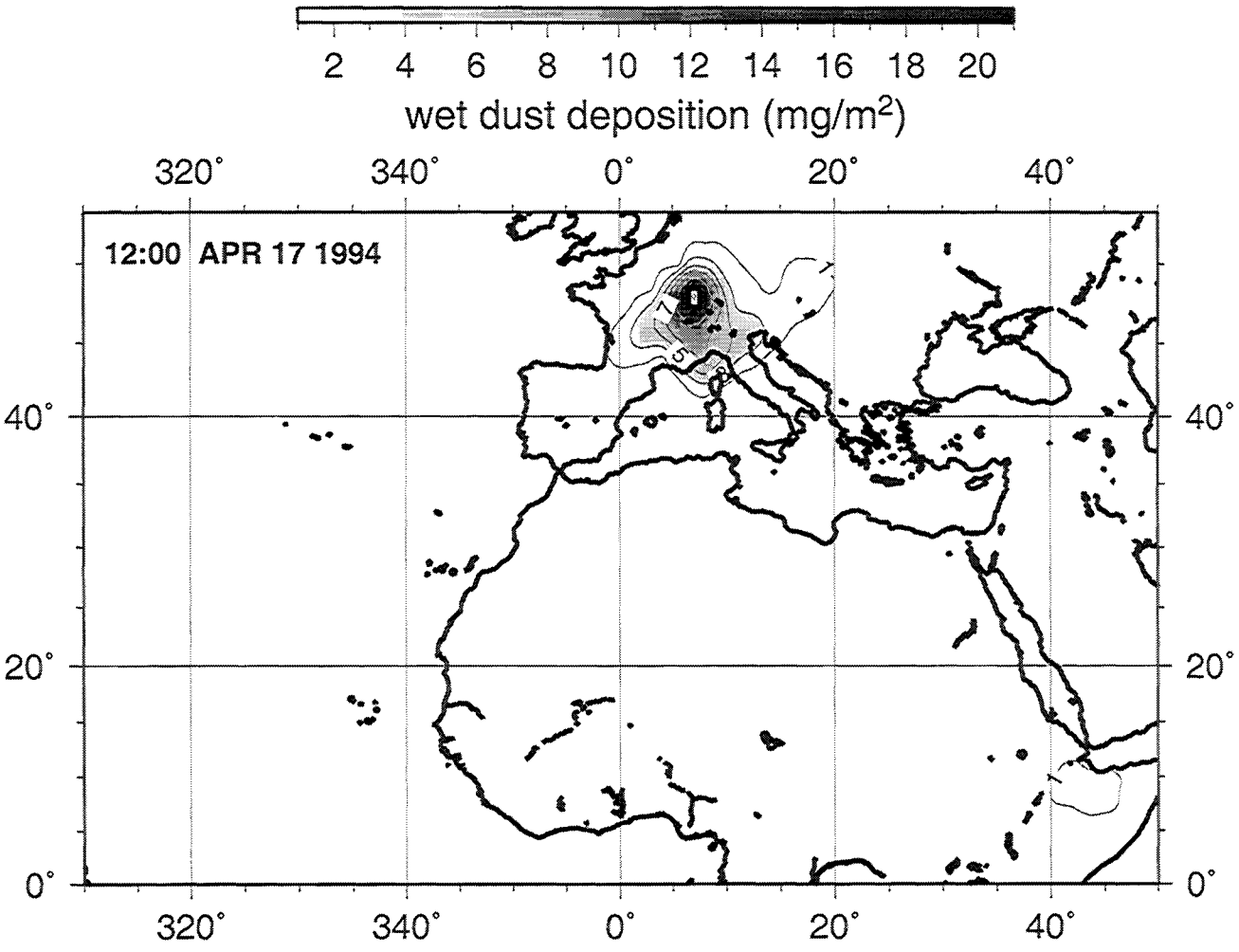
2 4 6 8 10 12 14 16 18 20
wet dust deposition (mg/m2)
320° 340° 0° 20° 40°
12:00 APR 17 1994
40°
20°
0°

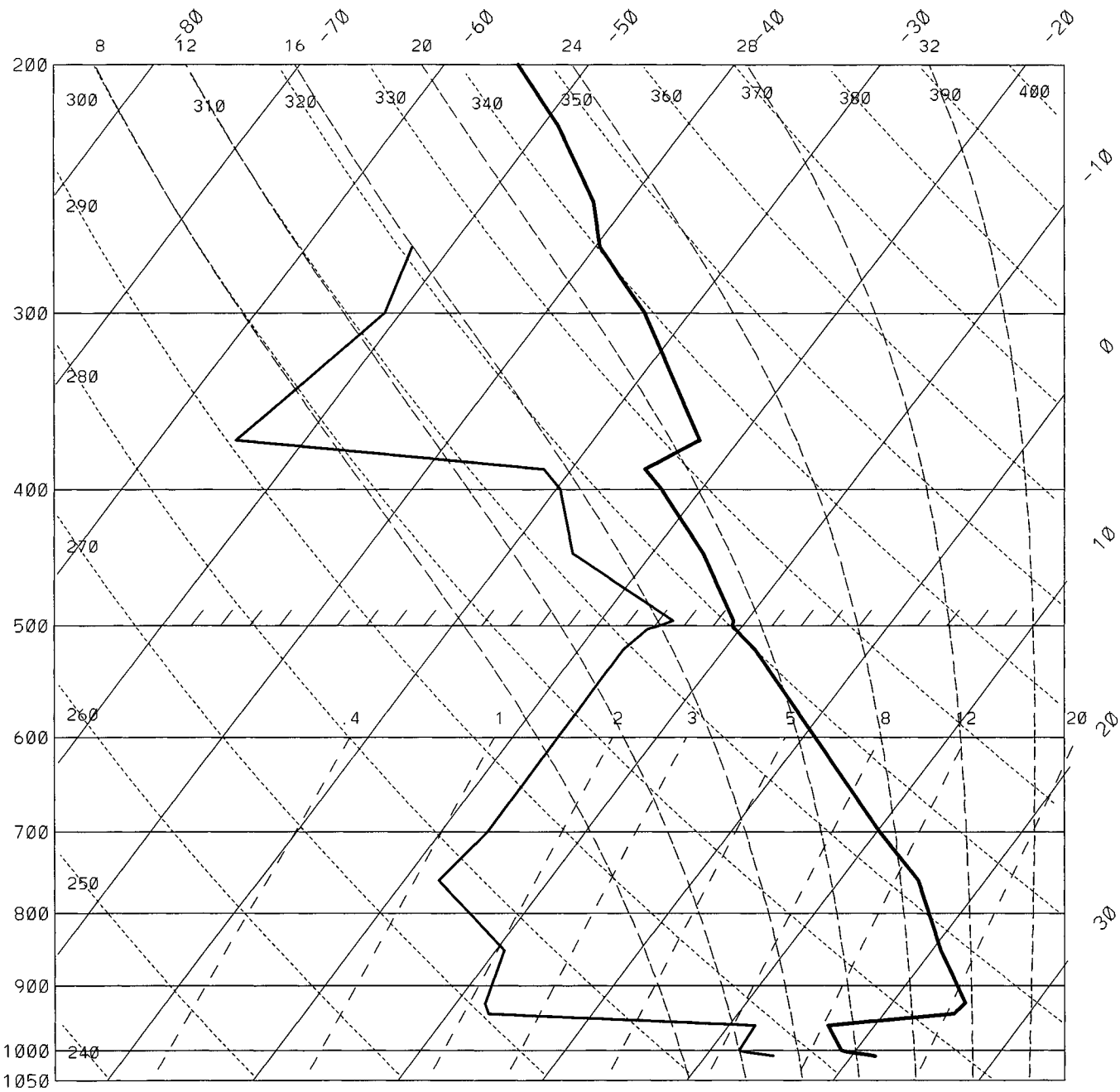

sounding at station: 8594 94 4 4 12 utc SAL ISLAND

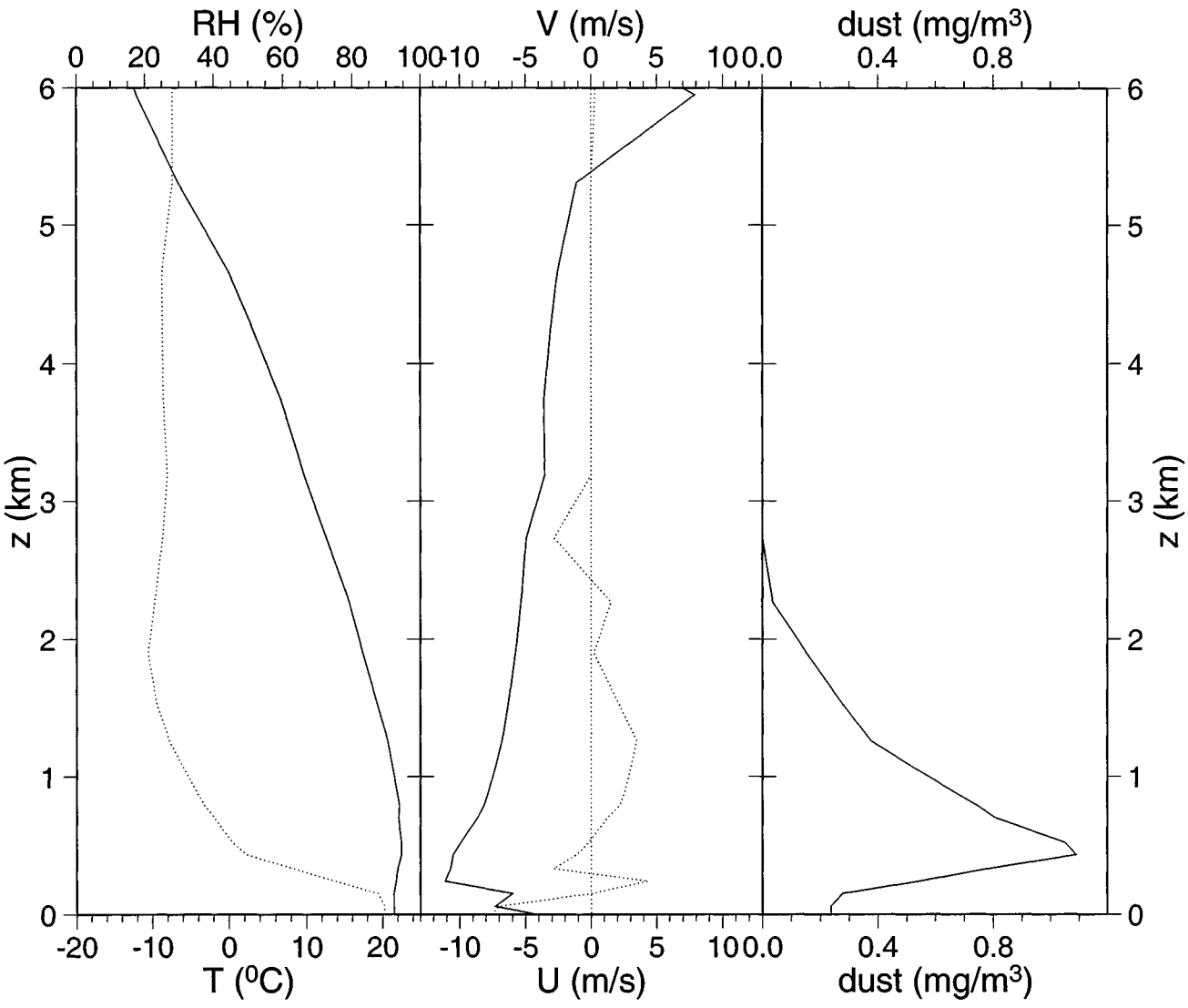
RH (%)
0 20 40 60 80 100
V (m/s)
-10 -5 0 5 10
dust (mg/m3)
0.0 0.4 0.8
z (km)
0 1 2 3 4 5 6
T (0C)
-20 -10 0 10 20
U (m/s)
-10 -5 0 5 10
dust (mg/m3)
0.0 0.4 0.8

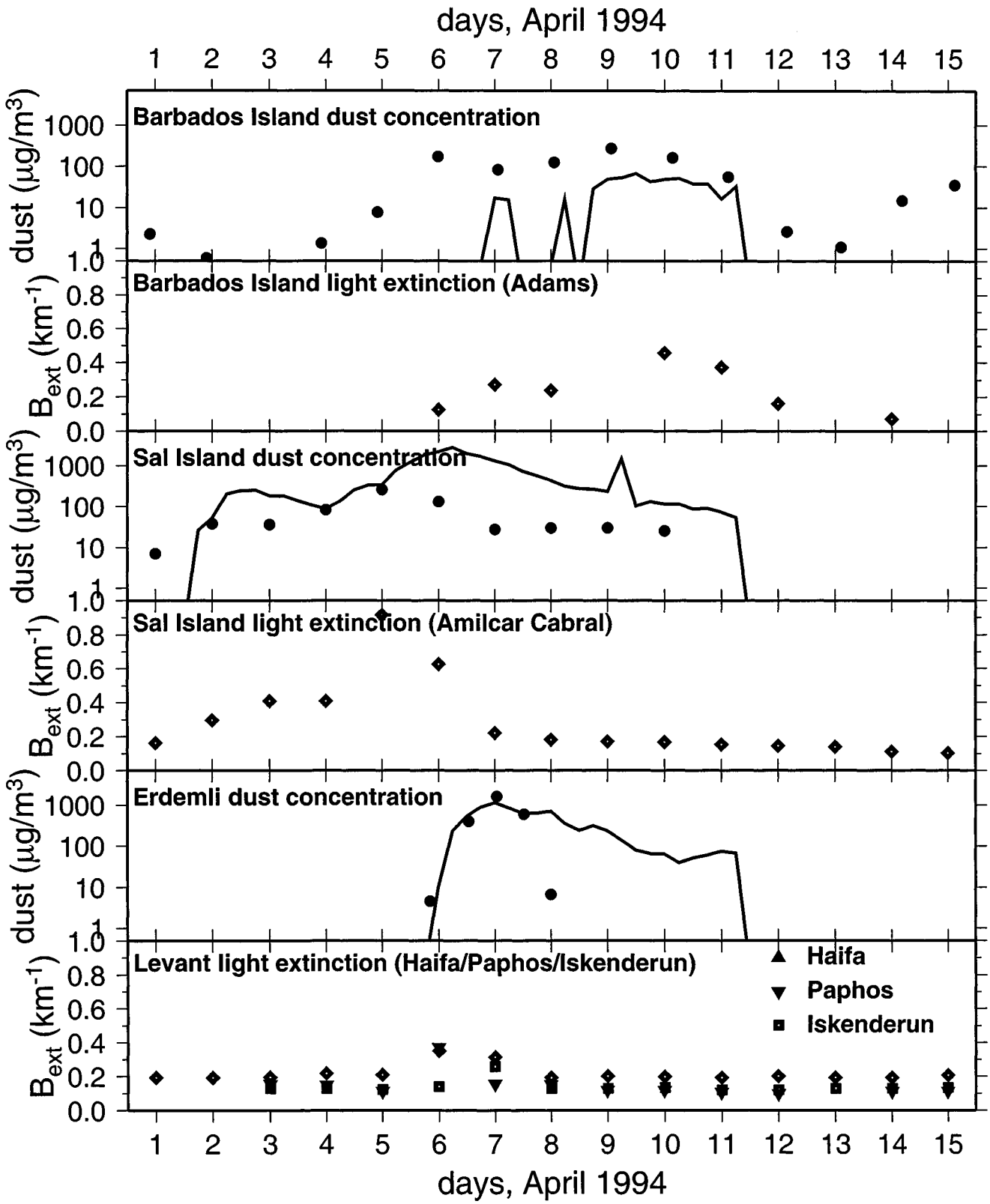
days, April 1994
1 2 3 4 5 6 7 8 9 10 11 12 13 14 15
Barbados Island dust concentration
dust (µg/m3)
1000
100
10
1
1.0
Barbados Island light extinction (Adams)
Bext (km-1)
0.8
0.6
0.4
0.2
0.0
Sal Island dust concentration
Sal Island light extinction (Amilcar Cabral)
Erdemli dust concentration
Levant light extinction (Haifa/Paphos/Iskenderun)
Haifa
Paphos
Iskenderun
days, April 1994

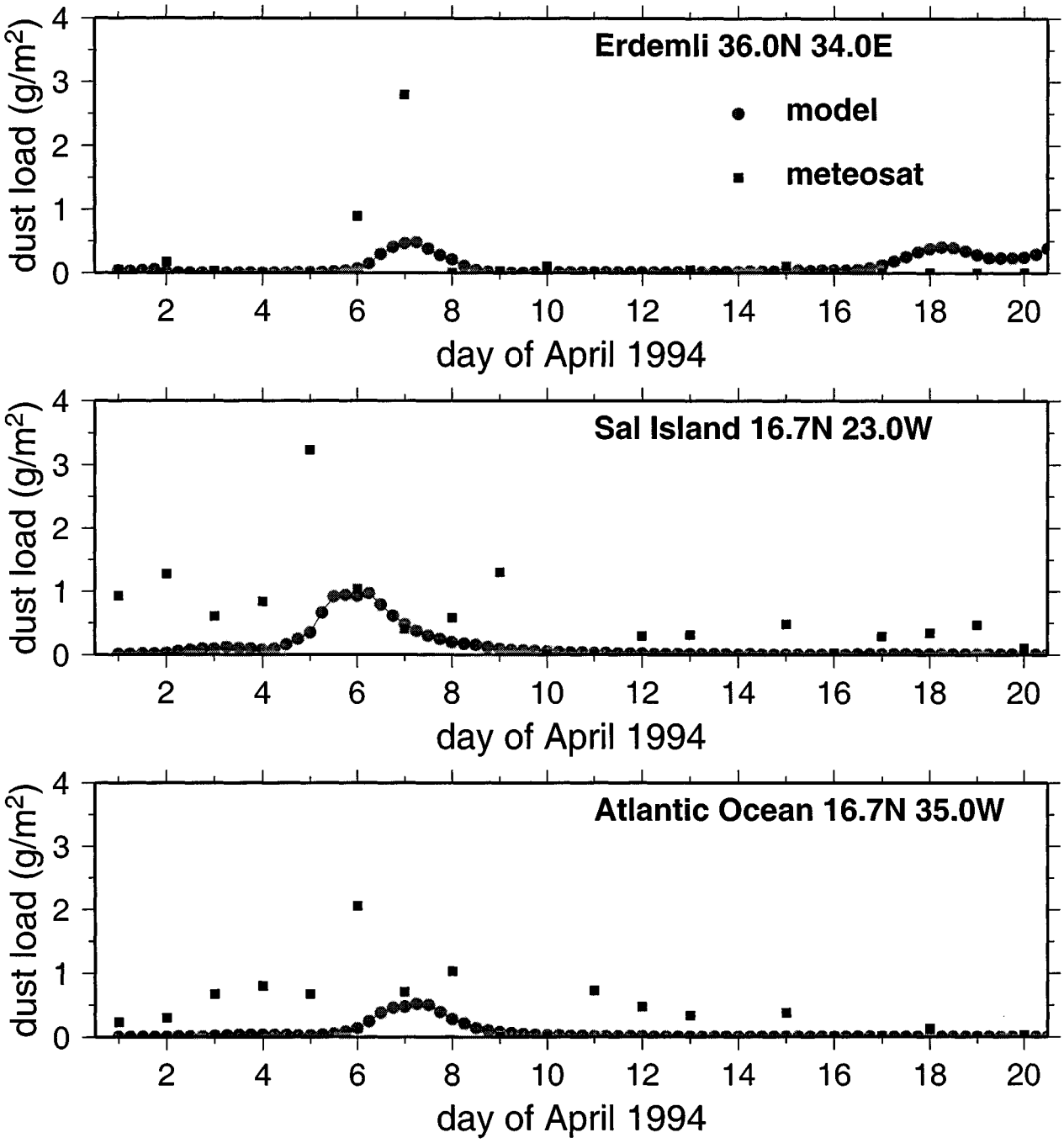
Erdemli 36.0N 34.0E
model
meteosat
dust load (g/m²)
day of April 1994
Sal Island 16.7N 23.0W
dust load (g/m²)
day of April 1994
Atlantic Ocean 16.7N 35.0W
dust load (g/m²)
day of April 1994

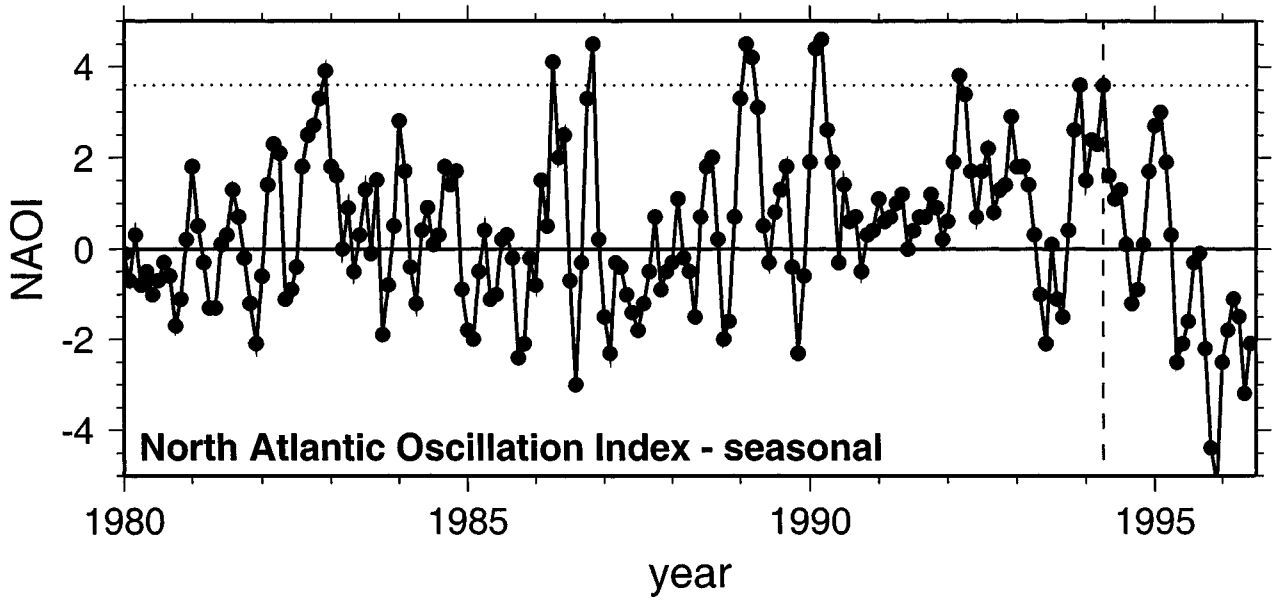
NAOI
4
2
0
-2
-4
North Atlantic Oscillation Index - seasonal
1980
1985
1990
1995
year